High-Power, Low-Noise 1.5-μm Slab-Coupled Optical Waveguide (SCOW) Emitters: Physics, Devices, and Applications

Paul W. Juodawlkis, *Senior Member, IEEE*, Jason J. Plant, William Loh, Leo J. Missaggia, Frederick J. O'Donnell, Douglas C. Oakley, Antonio Napoleone, Jonathan Klamkin, Juliet T. Gopinath, Daniel J. Ripin, Sangyoun Gee, Peter J. Delfyett, *Fellow, IEEE*, and Joseph P. Donnelly, *Life Fellow, IEEE*

(Invited Paper)

***Abstract*—We review the development of a new class of high-power, edge-emitting, semiconductor optical gain medium based on the slab-coupled optical waveguide (SCOW) concept. We restrict the scope to InP-based devices incorporating either InGaAsP or InGaAlAs quantum-well active regions and operating in the 1.5-μm-wavelength region. Key properties of the SCOW gain medium include large transverse optical mode dimensions (>5 × 5 μm), ultralow optical confinement factor ($\Gamma \sim$ 0.25–1%), and small internal loss coefficient ($\alpha_i \sim 0.5\,\mathrm{cm}^{-1}$). These properties have enabled the realization of 1) packaged Watt-class semiconductor optical amplifers (SOAs) having low-noise figure (4–5 dB), 2) monolithic passively mode-locked lasers generating 0.25-W average output power, 3) external-cavity fiber-ring actively mode-locked lasers exhibiting residual timing jitter of <10 fs (1 Hz to Nyquist), and 4) single-frequency external-cavity lasers producing 0.37-W output power with Gaussian (Lorentzian) linewidth of 35 kHz (1.75 kHz) and relative intensity noise (RIN) < −160 dB/Hz from 200 kHz to 10 GHz. We provide an overview the SCOW design principles, describe simulation results that quantify the performance limitations due to confinement factor, linear optical loss mechanisms, and nonlinear two-photon absorption (TPA) loss, and review the SCOW devices that have been demonstrated and applications that these devices are expected to enable.**

***Index Terms*—External-cavity lasers, mode-locked lasers, noise figure, optical waveguides, power amplifiers, quantum-well devices, semiconductor optical amplifiers, single-frequency lasers.**

I. Introduction

WATT-CLASS, low-noise optical amplifiers are required for a variety of applications including free-space optical communications, laser radar and imaging, high-performance microwave photonic (MWP) links and analog signal processors, and low-noise mode-locked lasers for photonic analog-to-digital converters and optical metrology based on optical frequency combs. Historically, applications requiring Watt-class optical amplifiers have utilized solid-state or doped-fiber gain media. For example, in the 1.5-μm-wavelength region, erbium-doped fiber amplifiers (EDFAs) generating greater than 150 W have been demonstrated [1] and 50-W EDFAs are available commercially [2]. Additionally, much of the work to develop low-noise femtosecond laser combs has utilized Ti-sapphire or other solid-state gain media, and EDFAs [3]–[5]. In addition to high-power, lasers based on solid-state and doped-fiber lasers have exhibited superior noise performance relative to semiconductor lasers due to their larger intracavity powers, smaller intracavity losses, and negligible gain/index coupling [6]. The main limitations of fiber and solid-state lasers is that their size and weight can be relatively large, and their power conversion efficiency is low (typically <10%) due to optical pumping inefficiencies.

A number of these applications could benefit from the use of semiconductor optical gain media if these media could have power and noise properties comparable to solid-state media. Benefits of semiconductor optical amplifiers (SOAs) relative to solid-state amplifiers include smaller size and weight, higher electrical-to-optical conversion efficiency, larger gain bandwidth, wavelength designability, and potential monolithic integration of SOAs with other components (e.g., lasers, modulators, detectors).

Traditional SOAs have been limited in both output power and noise performance. The primary factors limiting the output power of an SOA are the dimensions of the optical mode, the volume of the active region, the optical confinement factor Γ, which quantifies the spatial overlap between the optical mode and the active region, the electrical series resistance, and the thermal resistance which limits rate at which heat can be removed. The noise performance of SOAs has been limited by the internal loss coefficient α_i and large coupling loss.

In this paper, we review the physics and development of the slab-coupled optical waveguide (SCOW) gain medium, and describe SCOW-based emitters that have been realized in the 1.5-μm-wavelength region using InP quantum-well (QW) materials (see Fig. 1). The primary performance advances of the SCOW gain medium relative to previous waveguide SOAs are related to its large symmetric optical mode, small Γ, and small

Manuscript received December 14, 2010; revised February 14, 2011; accepted February 16, 2011. Date of publication April 25, 2011; date of current version December 7, 2011. This work was supported by the Defense Advanced Research Projects Agency under Air Force Contract FA8721–05-C-0002. Opinions, interpretations, conclusions, and recommendations are those of the authors, and are not necessarily endorsed by the United States Government.

P. W. Juodawlkis, J. J. Plant, W. Loh, L. J. Missaggia, F. J. O'Donnell, D. C. Oakley, A. Napoleone, J. Klamkin, D. J. Ripin, and J. P. Donnelly are with the Lincoln Laboratory, Massachusetts Institute of Technology, Lexington, MA 02420 USA (e-mail: juodawlkis@ll.mit.edu).

J. T. Gopinath is with the University of Colorado, Boulder, CO 80309 USA.

S. Gee and P. J. Delfyett are with the University of Central Florida, Orlando, FL 32816 USA.

Color versions of one or more of the figures in this paper are available online at http://ieeexplore.ieee.org.

Digital Object Identifier 10.1109/JSTQE.2011.2126041

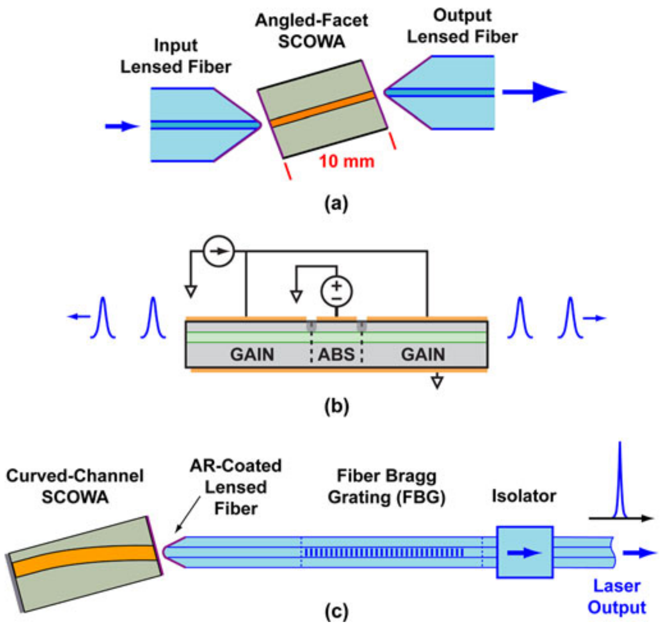

Fig. 1. Demonstrated applications of the slab-coupled optical waveguide (SCOW) gain medium: (a) traveling-wave SCOW amplifier (SCOWA), (b) colliding-pulse mode-locked SCOW laser (CPM-SCOWL), and (c) single-frequency SCOW external-cavity laser (SCOWECL).

α_i [7], [8]. We begin Section II with a review of three waveguide SOA architectures, including the SCOW amplifier [SCOWA, Fig. 1(a)], introduce several SOA performance parameters, and compare the reported performance parameters for the different SOA architectures. We then describe the SCOWA design principles and numerical simulations of steady-state SCOWA operation that have been developed to optimize SCOWA performance and to investigate performance limitations. Specifically, we summarize our discovery of the impact of nonlinear two-photon absorption (TPA) on the output power and efficiency of high-power SOAs. These simulations are directly compared to measurements of SCOWA gain, output power, and efficiency. SCOWA noise figure measurements and analysis are also discussed. In Section III, we describe the demonstration of SCOW-based mode-locked lasers. Passive mode-locked operation is obtained from monolithic devices using either fundamental or colliding-pulse mode-locking (CPM) geometries [Fig. 1(b)]. We also describe external-cavity actively mode-locked lasers incorporating SCOWA gain media with ultralow timing-jitter performance. In Section IV, we describe single-frequency SCOW external-cavity lasers [SCOWECLs, Fig. 1(c)] comprising double-pass, curved-channel SCOWAs and narrow-bandwidth fiber Bragg gratings (FBGs). We conclude the paper with discussion of potential applications and future directions.

II. SCOW Amplifiers (SCOWAs)

A. SOA Steady-State Performance Metrics

The steady-state performance of high-power SOAs is described by several parameters, including the small-signal gain (G_0), saturation output power ($P_{o,\mathrm{sat}}$), maximum output power ($P_{o,\max}$), electrical-to-optical conversion efficiency ($\eta_{e\text{-}o}$), and noise figure (*NF*). The small-signal gain is the net device gain when the input power is small enough so that the SOA operates in the unsaturated or linear region. It can be expressed as [9]

$$G_0 = \exp\left[(\Gamma g_0 - \alpha_i)\, L\right] \tag{1}$$

where $\Gamma = \Gamma_{\mathrm{xy}}$ is the transverse optical confinement factor, g_0 is the unsaturated active-material gain coefficient, α_i is the internal loss coefficient, and L *is* the length of the SOA. The saturation output power, defined as the output power where the amplifier gain G has decreased to half of the small-signal gain (i.e., $G = G_0/2$), can be written [9]

$$P_{\mathrm{o,sat}} = \left(\frac{G_0 \ln 2}{G_0 - 2}\right)\left(\frac{w\, d}{\Gamma}\right)\left(\frac{h\nu}{a\, \tau}\right) \tag{2}$$

where w and d are the width and thickness of the active material, respectively, $h\nu$ is the photon energy, a is the differential gain, and τ is the carrier lifetime. We note that (2) is an approximation that includes the following assumptions: 1) the material gain coefficient is linearly proportional to the carrier density, $g_0 = a(n_o - n_{TR})$, where n_o is steady-state carrier density under small-signal conditions and n_{TR} is the transparency carrier density, 2) a and τ are independent of the carrier density, and 3) $\alpha_i = 0$. We note that a more realistic quantum-well gain model having a logarithmic dependence on carrier density is used in the numerical simulations described in Section II-D. The maximum output power $P_{o,\max}$ of an SOA does not have a simple analytical expression as it depends on the gain saturation characteristic and the amount of input power available to drive the SOA. Obviously, the usefulness of an optical amplifier decreases as its net gain approaches 1.

The electrical-to-optical conversion efficiency $\eta_{e\text{-}o}$ of an SOA is defined as the added optical power divided by the input electrical input power and can be written as

$$\eta_{e\text{-}o} = \frac{P_{\mathrm{OUT}} - P_{\mathrm{IN}}}{P_{\mathrm{ELEC}}} = \frac{\eta_{c,\mathrm{out}} P_o \left(1 - (1/\eta_{c,\mathrm{in}}\eta_{c,\mathrm{out}} G)\right)}{I_{\mathrm{bias}}\, V_{\mathrm{bias}}} \tag{3}$$

where P_o is the optical power at the device output facet, G is the saturated device gain, $\eta_{c,\mathrm{in}}$ ($\eta_{c,\mathrm{out}}$) is the input (output) coupling efficiency, I_{bias} is the dc-bias current, and V_{bias} is the dc-bias voltage. We note that $\eta_{e\text{-}o}$ does not include the electrical power of any thermoelectric cooler (TEC) used to remove heat from the SOA. At a fixed electrical input power $P_{\mathrm{ELEC}} = I_{\mathrm{bias}} V_{\mathrm{bias}}$, (3) shows that the maximum $\eta_{e\text{-}o}$ occurs when P_o is large, but before the saturated gain becomes too small. This occurs when P_o is slightly larger than $P_{o,\mathrm{sat}}$ as will be shown later. To achieve high $\eta_{e\text{-}o}$, the coupling efficiencies should be large and G_0 should be large enough to ensure that $\eta_{c,\mathrm{in}}\eta_{c,\mathrm{out}} G_0 \gg 1$ since $G \le G_0$.

The noise figure (NF) of a SOA is given by [10]

$$\mathrm{NF} = \frac{1}{\eta_{c,\mathrm{in}}} \frac{2n_{\mathrm{sp}}(G-1)}{G} \frac{\Gamma g}{\Gamma g - \alpha_i} + \frac{1}{\eta_{c,\mathrm{in}}\eta_{c,\mathrm{out}} G} \tag{4}$$

where n_{sp} is the population inversion factor, and g is the saturated active-material gain coefficient. Low-noise figure is obtained through high coupling efficiency, high population inversion ($n_{\mathrm{sp}} \sim 1$), and low relative optical loss ($\Gamma g \gg \alpha_i$).

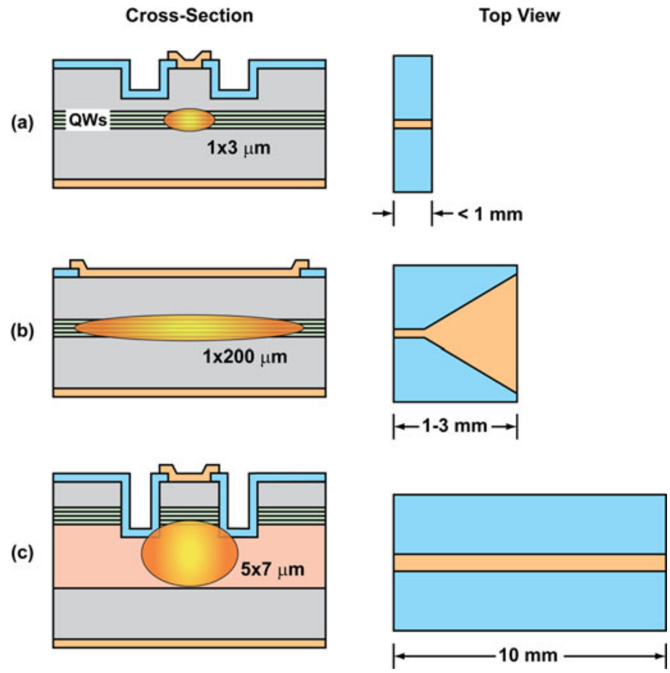

Fig. 2. Transverse cross-section and top-view schematics of waveguide semiconductor optical amplifiers (SOAs): (a) conventional rib-waveguide amplifier, (b) tapered-output amplifier, and (c) slab-coupled optical waveguide amplifier (SCOWA).

As expected, the *NF* is directly impacted by the input coupling loss $1/\eta_{c,\mathrm{in}}$. In the limit, the minimum is $NF \sim 2n_{\mathrm{sp}} = 2$ (3 dB).

B. SOA Architectures

A number of waveguide SOA architectures have been demonstrated [11]–[14]. Fig. 2 shows cross-section and top-view schematics of three classes of quantum-well waveguide SOA: (a) a conventional rib-waveguide structure, (b) a tapered-output amplifier, and (c) a slab-coupled optical waveguide amplifier (SCOWA). The primary differences between these waveguide SOA classes are the dimensions of the transverse optical mode, the transverse optical confinement factor Γ, the internal loss coefficient α_i, and the length L of the SOA.

The design of the conventional rib-waveguide SOA [Fig. 2(a)] is a direct reflection of the design of high-gain, high-speed directly modulated semiconductor lasers that were developed for the telecommunications industry [9], [15]. Indeed, early SOAs, also referred to as semiconductor laser amplifiers (SLAs), were simply telecom laser structures incorporating anti-reflection (AR) coated and/or angled facets to suppress lasing [11], [13]. In these SOAs, optical confinement in the vertical and lateral directions is obtained using a separate confinement heterostructure (SCH) region and an etched rib-waveguide, respectively. To maintain single-transverse-mode operation, both the SCH region thickness and the rib-waveguide width are kept fairly small and the resulting mode dimensions are on the order of 1×3 μm. High-speed laser modulation is obtained with a short length L and large Γ [9]. Therefore, these laser-based SOAs have typical lengths of L $<$ 1 mm and $\Gamma = 5$–20%. Since Γg is large in these structures, fairly large losses can be tolerated ($\alpha_i = 3$–$10\,\mathrm{cm}^{-1}$) before significantly impacting G_0, $\eta_{e\text{-}o}$, and *NF*.

Equation (2) shows that the saturation output power $P_{o,\mathrm{sat}}$ of an SOA can be increased by a combination of 1) increasing the area wd of the active region, 2) reducing the optical confinement factor Γ, and 3) reducing the differential gain a. The tapered-output SOA [Fig. 2(b)] is one approach to increase $P_{o,\mathrm{sat}}$ by increasing the width w of the active region [see (2)] [16], [17]. Tapered InGaAsP QW SOAs, with w of a few hundred microns, have been reported with output powers of 0.3 W at 1.5 μm (1% duty cycle) [18] and 0.75 W at 1.3 μm [19]. Although capable of high power, tapered SOAs are limited by beam instability associated with gain guiding dynamics, filamentation, and by complex optics required to efficiently couple to single-mode optical fibers. Typical tapered-SOA to single-mode-fiber coupling efficiencies are about 50%. Tapered-output SOAs usually have Γ and α_i similar to rib-waveguide SOAs.

A second approach to increase $P_{o,\mathrm{sat}}$ is to decrease Γ. It has been shown that both Γ and α_i are reduced by increasing the thickness of the optical waveguide [20]–[22]. By reducing Γ to $\sim$1%, $P_{o,\mathrm{sat}} = 0.25$ W and small-signal gain $G_0 = 13$ dB was obtained from an InGaAsP quantum-well (QW) SOA device at 1590 nm [23]. Other groups have reported InGaAsP QW SOAs having $P_{o,\mathrm{sat}} \sim 0.1$ W through the use of low-Γ structures [24], [25]. In a conventional SOA or semiconductor laser structure, the maximum waveguide thickness is limited by the generation of higher-order transverse modes that compete for gain with the desired fundamental mode.

The SCOWA geometry [Fig. 2(c)] represents a significant advance over prior low-Γ SOA designs due to its larger optical mode size, smaller Γ, and smaller α_i. The SCOW concept is based on Marcatilli's observation that a multimode waveguide can be made to operate single mode by coupling the multimode waveguide to a slab waveguide [26]. By choosing the appropriate dimensions and coupling between waveguides, the fundamental mode will propagate with minimum loss while the higher-order modes will radiate away into the slab with high loss. We initially combined this waveguide concept with modern quantum-well technology to develop a new class of semiconductor laser, referred to as a slab-coupled optical waveguide laser (SCOWL) that supports a large fundamental transverse mode and has low optical loss ($<1\,\mathrm{cm}^{-1}$), allowing it to be long, thereby enabling efficient heat removal. The low internal loss coefficient is achieved by designing the structure to have small overlap between the optical mode and the lossy p-doped cladding layer. The initial demonstration of the SCOWL concept was reported by Walpole *et al.* at a wavelength of 1300 nm [27]. We have since demonstrated SCOWL operation at a variety of wavelengths (915, 980, 1060, 1550, and 2200 nm) with CW output powers ranging from 0.6 to 1.8 W and laser-to-fiber butt-coupling efficiency in excess of 80% [28]–[31].

For SOAs, (1) and (2) reveal a Γ-dependent tradeoff between G_0 and $P_{o,\mathrm{sat}}$. The amount by which Γ can be reduced to increase $P_{o,\mathrm{sat}}$ is limited by the decrease in modal gain that also occurs as Γ is reduced. The net gain coefficient of a waveguide SOA can be written as $g_{\mathrm{net}} = \Gamma g - \alpha_i(\mathrm{cm}^{-1})$. To obtain useful optical gain from a low-Γ SOA, α_i must be kept smaller than

Γg and the SOA length must increase as $g_{\rm net}$ decreases. Several loss mechanisms contribute to α_i, including free-carrier absorption (FCA) associated with carriers in the doped waveguide and cladding regions, FCA associated with injected carriers in the active region, waveguide scattering losses, and two-photon absorption (TPA) and FCA associated with TPA-generated carriers. By centering the optical mode in a relatively low-doped n-type InGaAsP waveguide and grading the p- and n-doping profiles, we have been able to achieve $\alpha_i \sim 0.5\,\text{cm}^{-1}$ in InGaAsP QW SCOWLs at threshold current conditions [30].

The tradeoff between G_0 and $P_{o,\rm sat}$, can be quantified by defining a gain-power (*G•P*) product that is independent of Γ. An approximate *G•P* product with units of W-dB can be obtained by 1) combining (1) and (2) with (2) expressed in decibels, 2) assuming that $G_0 \gg 1$, and 3) setting $\alpha_i = 0$ [32]

$$G \bullet P = G_{0,\rm dB} \cdot P_{o,\rm sat} \approx 3\,h\nu \left(\frac{\eta_o^d\, I_{\rm bias}}{q} - \frac{w\,d\,L}{\tau} n_{TR} \right) \quad (5)$$

where η_o^d is the internal differential efficiency [33], $I_{\rm bias}$ is the dc-bias current, and q is the electronic charge. In deriving (5), we have substituted in the linear expression for g_0 and the steady-state carrier-density n. We note that *G•P* is also independent of a. The *G•P* product allows the tradeoff between $P_{o,\rm sat}$ and G_0 to be evaluated in terms of device design and operating parameters. For the SCOWA-relevant example when $I_{\rm bias} = 5$ A and $\lambda = 1540$ nm, the maximum value that (3) can attain (i.e., $\eta_o^d = 1$, $n_{TR} = 0$) is 12 W-dB. This implies that if Γ is adjusted to obtain $P_{o,\rm sat} = 1$ W, the maximum achievable gain under these conditions is $G_0 = 12$ dB. We note that (5) is only approximate and tends to underestimate the *G•P* product due to the simplifying assumptions in its derivation.

In all of the above discussion, the SOA architectures utilized QW active regions. We note that the use of semiconductor quantum-dot (QD) active regions would likely benefit low-Γ SOAs such as the SCOWA. SOAs based on InAs/InP QDs have demonstrated device $P_{o,\rm sat} = 0.37$ W at 1.5 μm [34], [35]. To our knowledge, these QD results represent the highest output powers from fundamental-mode SOA devices reported by other groups. The high value of $P_{o,\rm sat}$ in QD SOAs is due to a combination of small confinement ($\Gamma < 1\%$) and small differential gain at high-injection current [36].

C. SCOWA Design and Fabrication Details

The SCOW amplifier designs are based on the SCOW laser designs that were initially demonstrated [27], [28]. Figs. 3 and 4 show a transverse cross-section and a generic material structure, respectively, that are common to most of the 1.5-μm QW SCOW emitters that have been demonstrated. To date all of our 1.5-μm SCOW emitter structures have been grown via organometallic vapor-phase epitaxy (OMVPE) on an n-type (100) InP substrate. With the exception of some early work where a h = 4 μm waveguide was investigated [30], all of the structures have used a h = 5 μm lightly n-type doped InGaAsP waveguide (5×10^{16} cm^{-3}, $\lambda_g = 1.03$ μm). Both InGaAsP and InGaAlAs QW active regions have been explored with the number of QWs ranging from 3 to 5. The well layers have been compressively

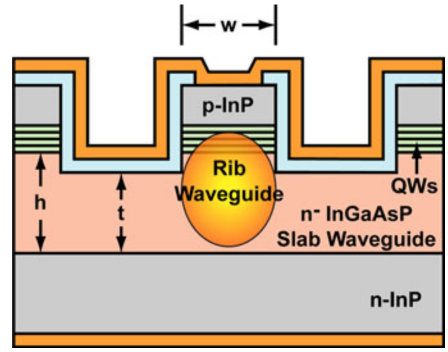

Fig. 3. Transverse cross-section of an InGaAsP/InP quantum-well slab-coupled optical waveguide amplifier (SCOWA) showing critical device dimensions.

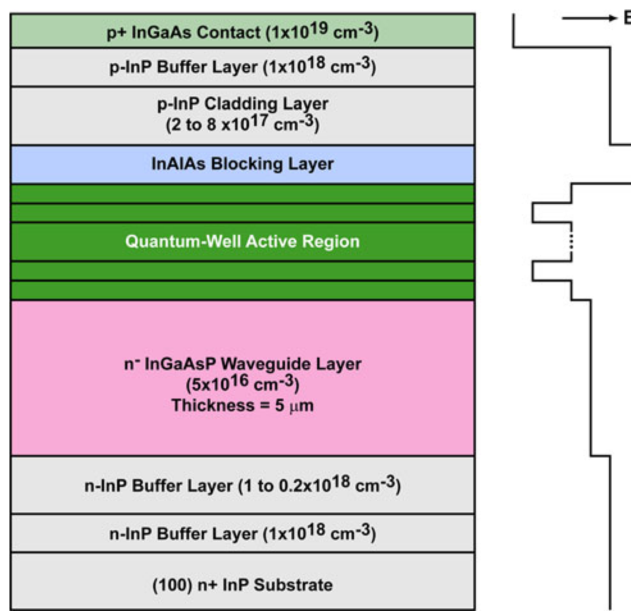

Fig. 4. Generic material layer structure for 1.5-μm InP-based SCOW gain medium. Schematic conduction-band energy diagram also shown.

strained (+1%) and the barrier and bounding layers have been tensile strained (−0.3%). Due to the weak confinement in the SCOW structure, Γ is strongly dependent on the effective index of the QW region. This effective index is determined by the composition of the QW and barrier layers, the number and thickness of the QWs, the thickness of the barrier layers, and the composition and thickness of the bounding layers. Some of the structures incorporated a thin (15 to 25 nm) p-doped InAlAs electron-blocking layer to minimize the impact of carrier leakage from the QW region into the p-InP cladding layer. We note that we did not observe a significant difference in performance for devices with an InAlAs electron-blocking layer relative to devices without the layer. The QW region and waveguide layer are sandwiched between p- and n-InP cladding layers with graded doping. To minimize the optical loss associated with FCA, the doping of the cladding layers was graded from approximately 2×10^{17} cm^{-3} near the waveguide to 10^{18} cm^{-3} away from the waveguide. A p+InGaAs layer was grown on the top of the p-InP buffer layer to enable low contact resistance.

Lateral optical confinement was obtained by reactive-ion etching a strip-loaded rib waveguide (w ~5.5 to 6 μm) to an appropriate depth of ~0.5 μm into the 5-μm-thick InGaAsP waveguide layer below the quantum wells. A SiO_2 layer was deposited for electrical isolation. The p- (Ti/Pt/Au) and n-contacts (Ni/Ge/Au) were deposited via e-beam evaporation and simultaneously alloyed at 450°C for 30 s. For amplifier structures, the facet reflectivity was minimized by a combination of 5°-oriented (110) angle cleaving followed by anti-reflection coating. The typical cleaved device length was 10 mm.

D. SCOWA Simulations

To understand and optimize the performance of the low-Γ SCOWA architecture, we have developed a numerical simulation based on a steady-state SOA model [37]. In the simulation, the SOA is divided into M sections along its length. A proportional fraction of the total bias current is injected into each section. In each section, rate equations are solved self consistently to determine the carrier density and optical signal power as a function of injection current and input optical power. The carrier lifetime τ has the standard form $1/\tau = A + Bn + Cn^2$. For the InGaAsP QWs modeled here we used the parameters [38], [39]: $A = 1.1 \times 10^8$ s^{-1}, $B = 2.2 \times 10^{-10} - (4 \times 10^{-29})\cdot n$ cm^{3}s^{-1}, and $C = 1 \times 10^{-28}$ cm^{6}s^{-1}.

In the model, the single-QW material gain coefficient is $g(n) = g_i \ln[(n + n_S) / (n_{TR} + n_S)]$, where n is the injected QW carrier density, $g_i = 415$ cm^{-1}, $n_{TR} = 1.65 \times 10^{18}$ cm^{-3} is the transparency carrier density, and $n_S = -1.43 \times 10^{18}$ cm^{-3} is an additional fitting parameter [38]. The values of g_i, n_{TR}, and n_S were determined from the measured small-signal gain of a packaged SCOWA [8] at 1540 nm at several bias currents. Estimation of the carrier density n from the injected current density was obtained by solving the carrier-density rate equations under the small-signal, steady-state condition. The simulated optical mode was a 2-D Gaussian distribution with 1/e^2-intensity mode widths of 5 and 7 μm in the vertical and lateral directions, respectively. Other important SCOWA simulation parameters are the optical confinement factor $\Gamma = 0.5\%$, waveguide width $w = 5.7$ μm, active region thickness $d = 40$ nm $= 5 \times 8$-nm QWs, length L = 10 mm, and fiber-to-waveguide coupling efficiency $\eta_C = 90\%$.

The diode turn-on voltage and series resistance used in the simulation were 0.89 V and 0.12 Ω, respectively, which are typical values for a 10-mm-long SCOWA as determined from a four-point current-voltage (I-V) measurement. The series resistance is comprised of the resistance of the waveguide layer, the cladding layers, and the metal-semiconductor contact resistances. The dominant component is attributed to the resistance of the p-InP cladding layer, which has a graded doping profile to minimize the optical loss due to FCA (see above). The trade-off between series resistance and optical loss due to the doping of the cladding and waveguide layers is more pronounced in the SCOWAs relative to conventional SOAs due to the inherent requirement of low optical loss in the low-Γ SCOWA design.

Comparison of the simulated and measured gain saturation characteristics of 1.5-μm SCOWAs has led us to discover that

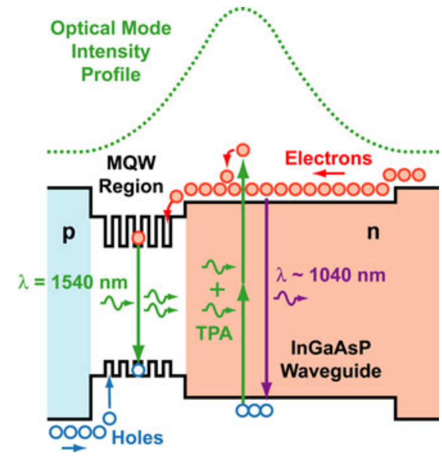

Fig. 5. Band-diagram schematic of multiple quantum well (MQW) p-i-n SCOWA structure depicting electronic carrier injection, stimulated emission of fundamental (1540 nm) signal, generation of carriers in the waveguide region via two-photon absorption (TPA), and 1040-nm radiative recombination of TPA-generated carriers.

the CW output intensity of low-Γ SOAs and lasers can be limited by nonlinear optical loss due to two-photon absorption (TPA) and the FCA associated with the TPA-generated carriers [40]. The SCOWA band-diagram schematic in Fig. 5 summarizes our interpretation of the TPA and TPA-generated FCA physics. Under forward-bias, electrons and holes are injected into the SCOWA's QW region from the n-doped waveguide and p-doped cladding region, respectively. When the QW carrier density is large enough to provide gain, optical signals injected into the SCOWA at wavelengths within the gain bandwidth are amplified through stimulated emission. In the SCOWA design, most of the optical mode is confined to the waveguide region and it has only a small overlap with the QW region. When the amplified signal power becomes large, electron-hole pairs are generated via TPA in the waveguide where the mode intensity is largest. This TPA mechanism acts to directly deplete the optical field. The TPA-generated carriers, primarily the holes, introduce an additional loss mechanism through FCA. The TPA and TPA-generated FCA optical loss mechanisms limit the maximum intensity that can be produced by the amplifier. We have confirmed the presence of the TPA-generated carriers in a SCOWA by observing photoluminescence at the wavelength corresponding to the bandgap wavelength (~1040 nm) of the waveguide material [40]. The photoluminescence power has a quadratic dependence on the amplified SCOWA output power of an inband signal ($\lambda = 1540$ nm) as expected for a TPA process. We note that the photoluminescence is not due to the often-cited carrier spillover effect [41]–[43], since it is not present when the SCOWA optical input power is zero, even at high-bias current.

The impact of TPA and TPA-generated FCA is incorporated into the simulation through the internal loss coefficient, which is dependent on both the injected carrier density and the optical intensity

$$\alpha_i = \alpha_0 + \alpha_{\mathrm{QW}} + \alpha_2 + \alpha_{2\mathrm{FCA}} \tag{6}$$

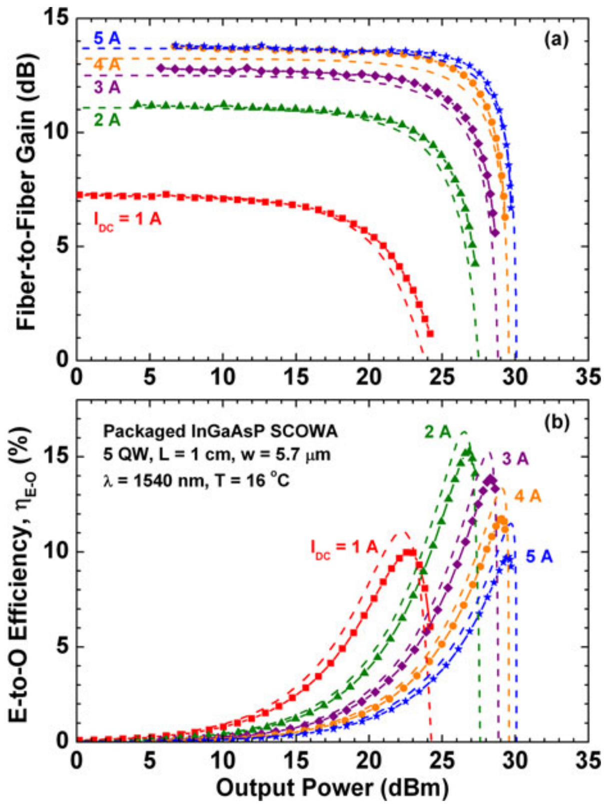

Fig. 6. Comparison of measured (symbols) and simulated (dotted lines) characteristics of a packaged InGaAsP/InP QW SCOWA as a function of output power at several bias currents: (a) fiber-to-fiber gain, (b) electrical-to-optical conversion efficiency.

where α_0 is the carrier-independent loss, $\alpha_{\rm QW} = \Gamma\,\sigma_{\rm IVBA}\,p$ is the intervalence-band absorption (IVBA) loss due to injected holes in the QW layers, $\sigma_{\rm IVBA} = 7.5 \times 10^{-17}$ cm^2 is IVBA cross-section, p is the hole density in the QWs (assume uniform distribution and $n = p$), α_2 is the TPA absorption coefficient given by

$$\alpha_2 = \beta_{\rm TPA} \cdot I_S \tag{7}$$

where $\beta_{\rm TPA} = 60$ cm/W is the TPA coefficient, I_S is the effective optical signal intensity, $\alpha_{\rm 2FCA}$ is the absorption coefficient due to TPA-generated FCA which can be written in steady state as

$$\alpha_{\rm 2FCA} = \sigma_{\rm 2FCA} \cdot \left(\frac{\beta_{\rm TPA}\, I_S^2\, \tau_2}{h\nu}\right) \tag{8}$$

where $\sigma_{\rm 2FCA} = 7 \times 10^{-17}$ cm^2 is the FCA cross-section of the TPA-generated carriers, $h\nu$ is the photon energy of the fundamental optical signal, and $\tau_2 = 2.3$ ns is the lifetime of the TPA-generated carriers. The values of $\beta_{\rm TPA}$ and $\sigma_{\rm 2FCA}$ agree with values derived from ultrafast pump-probe measurements performed on a SCOWA [44]. The value of τ_2 was chosen to obtain agreement between the simulated and measured values of $P_{o,\rm sat}$ at a 5-A bias current.

Comparisons of the simulated and measured gain and efficiency characteristics of a packaged SCOWA amplifier [8] are provided in Fig. 6. The only parameter that was varied in generating the five simulated curves in each of these plots was the dc-bias current. All other simulation parameters were held fixed. The data of Fig. 6(a) reveal excellent agreement between the simulated and measured gain-saturation characteristics. We expect good agreement between the small-signal gain values since the simulation's material-gain coefficient expression is derived from measured small-signal gain data. The strong clamping of the small-signal gain versus bias current is likely due to increased IVBA associated with holes either confined in the QWs or thermalized into the barrier or cladding layers [41], [45]. The effect of this gain clamping is incorporated into the simulation through the material gain coefficient *g(n)* that was determined from measured small-signal gain versus current data as described above. In addition to the agreement between the simulated and measured small-signal gain values, both the saturation output power $P_{o,\rm sat}$ values and the roll-off shapes of the gain-saturation curves are almost identical. When the effects of TPA and TPA-generated FCA are not included in the simulation [32], we were not able to obtain the correct roll-off shape at high output power. From the simulation, we estimate that the TPA and TPA-generated FCA coefficients are $\alpha_2 = 0.18$ and $\alpha_{\rm 2TPA} = 0.72\,{\rm cm}^{-1}$, respectively, at 5-A bias current and at $P_o = P_{o,\rm sat} = 0.8$ W. These results show that the nonlinear loss due to TPA-generated FCA is larger than the direct TPA loss. We also note that TPA effects are more evident in SOA structures like the SCOWA that have low intrinsic losses (i.e., α_0 and $\alpha_{\rm QW}$).

Excellent agreement is also obtained between the simulated and measured efficiency versus output power characteristics [Fig. 6(b)]. The efficiency is small for small output power and peaks at output power slightly greater than $P_{o,\rm sat}$. The maximum difference between the simulated and measured peak-efficiency for the different biases is about 1.7%. The maximum efficiency occurs for a 2-A bias and then decreases with increasing bias. We attribute the decrease in efficiency at higher-bias current to increased Auger recombination, and increased internal loss due to a combination of carrier-density-dependent FCA and optical-intensity-dependent TPA. We observe that the simulated peak efficiency at 5-A bias increases from 11.5% to 19.5% if the losses due to TPA and TPA-generated FCA are neglected.

Having established the validity of the steady-state SCOWA simulation, we can use it to predict the impact of varying both Γ and α_i on the performance of low-Γ SOA structures. Fig. 7 shows the simulated $P_{o,\rm sat}$ and maximum electrical-to-optical conversion efficiency $\eta_{e\text{-}o,\max}$ of a 10-mm-long InGaAsP/InP SCOWA ($I_{\rm bias} = 5$ A) as a function of Γ and the carrier-independent loss coefficient α_0. The results reveal that $P_{o,\rm sat}$ initially increases as Γ decreases as predicted by (2), but reaches a maximum and then begins to decrease with further decrease in Γ. This maximum and subsequent decrease in $P_{o,\rm sat}$ is a direct result of the limit due to TPA. We note the excellent agreement between the maximum value of $P_{o,\rm sat}$ predicted by the simulation (∼0.8–0.9 W) and the value measured for a SCOWA having $\Gamma \sim 0.5\%$ and $\alpha_i \sim 0.5\,{\rm cm}^{-1}$ [see Fig. 6(a)]. When TPA effects are not included in the simulation, $P_{o,\rm sat}$ increases without bound in direct accordance with (2). The maximum efficiency $\eta_{e\text{-}o,\max}$ is initially relatively independent of Γ and then begins to decrease as the output power

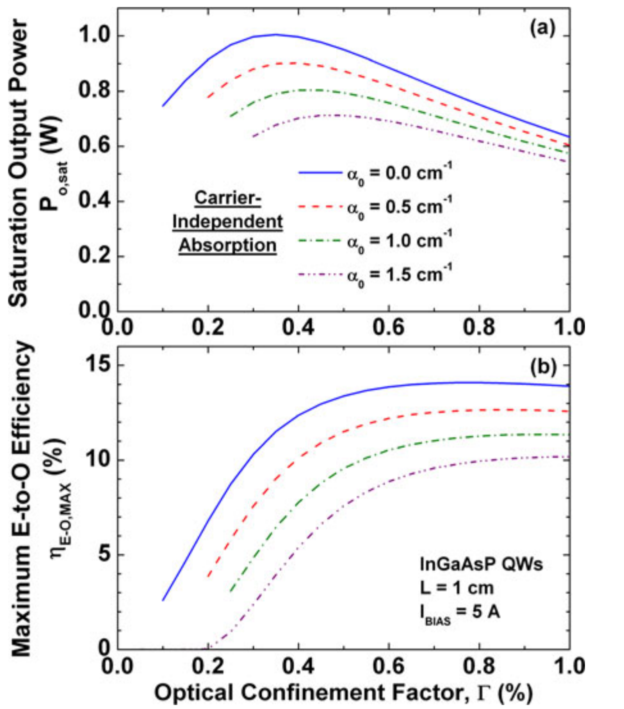

Fig. 7. Simulated (a) saturation output power $P_{o,\mathrm{sat}}$, and (b) maximum electrical-to-optical conversion efficiency $\eta_{e\text{-}o,\max}$ as a function of optical confinement factor Γ for different carrier-independent loss coefficients α_0.

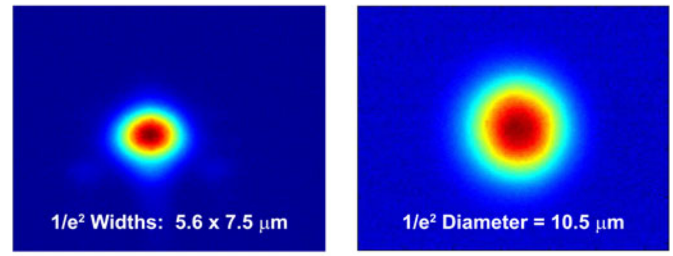

(a) (b)

Fig. 8. Measured near-field intensity mode-profiles of (a) 1.5-μm SCOWA, and (b) single-mode optical fiber (SMF-28).

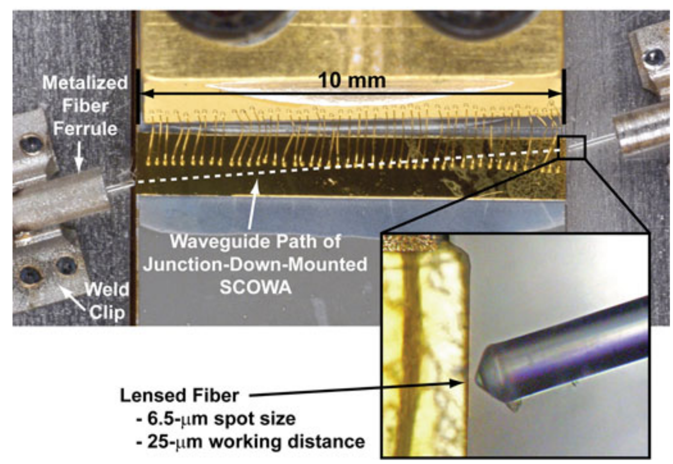

Fig. 9. Top-view photograph of junction-down-mounted SCOWA packaged using lensed-fiber pigtails. SCOWA length = 10 mm. SCOWA facet angle = 5 degrees. SCOWA soldered to Cu-W submount. Lensed-fiber parameters: fiber = SMF-28, spot size = 6.5 μm, working distance = 25 μm.

becomes limited by TPA and the gain decreases [see (1)]. Once again, the simulated efficiency value agrees well with the measured value [see Fig. 6(b)]. When TPA effects are not included, $\eta_{e\text{-}o,\max}$ increases from 12% to more than 18% for $\Gamma \sim 0.5\%$ and $\alpha_i \sim 0.5\,\mathrm{cm}^{-1}$. Multisection contacts can be used to increase the efficiency (see Section II-E below), but they do not mitigate the impact of TPA. The simulation results also show that both $P_{o,\mathrm{sat}}$ and $\eta_{e\text{-}o,\max}$ decrease with increasing optical loss.

E. SCOWA Demonstrations

The initial bench-top demonstration of an SOA based on the SCOW concept, performed at a wavelength of 1.5-μm, showed that more than 0.63 W of output power could be coupled into an SMF-28 optical fiber using simple butt-coupling [7]. The coupling efficiency between the SCOWA having a 5°-angled facet and the angled-facet SMF-28 fiber was measured to be ~55%.

Fig. 8 shows a comparison of the measured near-field mode profiles of a SCOWA and an SMF-28 fiber. Typical 1/e^2-intensity mode widths of the 1.5-μm SCOWAs are 4 to 6 μm in the vertical direction (perpendicular to the growth plane), and 7 to 8 μm in the lateral direction (parallel to the growth plane). Thus, the SCOWA mode area is 10 to 15 times larger than a conventional SOA having mode dimensions of 1 × 3 μm. Overlap integrals of measured mode profiles predict SCOWA to SMF-28 coupling efficiencies of 70–75%, while they have been measured to be 55–60%. We were also able to achieve SCOWA-to-fiber butt-coupling efficiency greater than 80% by using an optical fiber (HI1060 Flex) having a smaller mode size (1/e^2 diameter = 6.5 μm).

The SCOWA-to-fiber coupling efficiency was increased to more than 90% by using conical lensed SMF-28 fibers having a focus spot diameter of 6.5 μm. In addition to providing a near-optimal mode overlap, the lensed fibers have a 25-μm working distance, which allows the SCOWA-to-fiber separation to be optimized during the fiber alignment process. Fig. 9 shows a top-view photograph of a packaged SCOWA that was pigtailed using lensed SMF-28 fibers [8]. The SCOWA was mounted junction-side down to a Cu-W submount using AuSn solder. The submount was mounted to a Cu baseplate that was temperature controlled using a thermoelectric cooler. The input and output facets were coupled to the lensed fibers and affixed using laser welding. Prior to packaging, the 1/e^2 widths of the SCOWA near-field mode profile (Fig. 8) were measured to be 5.6 and 7.5 μm, perpendicular and parallel to the growth plane, respectively.

Fig. 10 shows the measured small-signal gain spectra of the packaged SCOWA. For these measurements, the input power was approximately 1 mW. At a bias current of 5 A and T = 16 °C, the peak fiber-to-fiber gain was 14.9 dB at 1500 nm and the 3-dB bandwidth was greater than 100 nm. The TE/TM gain ratio was measured to be 17–18 dB and was nearly independent

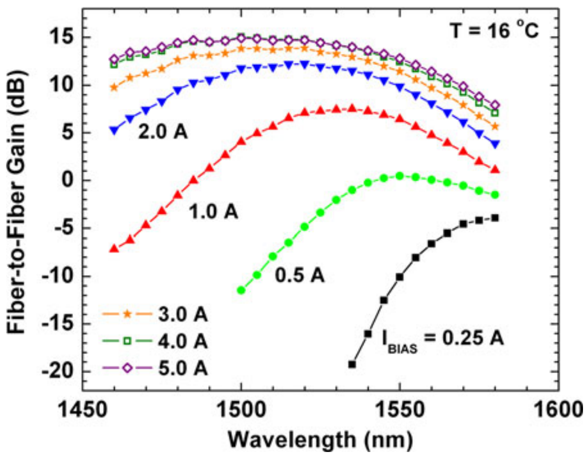

Fig. 10. Small-signal gain spectra of a packaged SCOWA for several bias currents. Baseplate temperature = 16 °C.

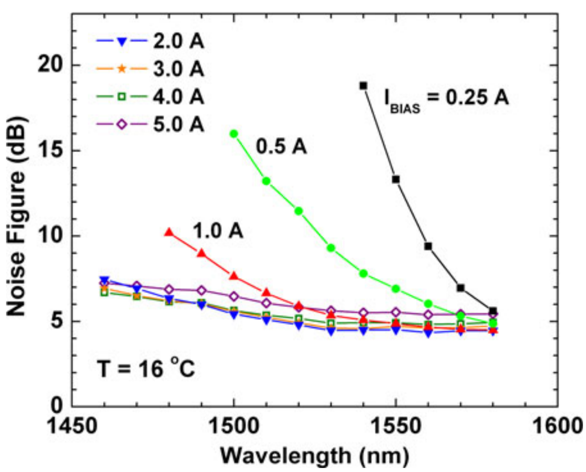

Fig. 11. Noise figure of a packaged SCOWA as a function of wavelength for several bias currents measured, using the optical source subtraction technique. Baseplate temperature = 16 °C.

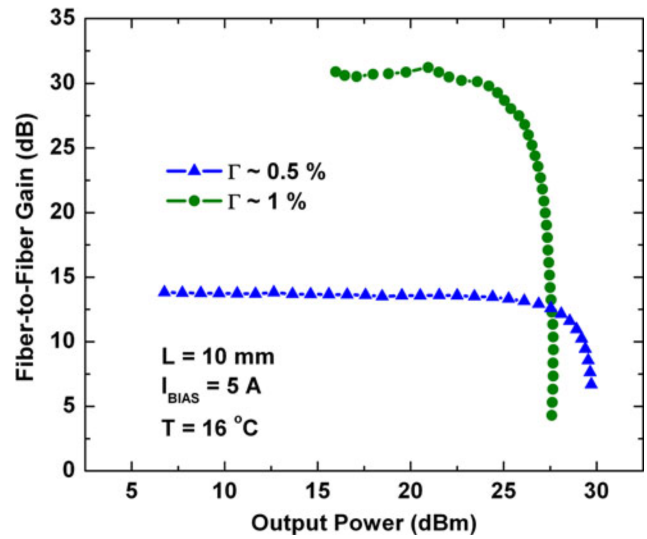

Fig. 12. Gain saturation characteristics of 10-mm-long packaged InGaAsP/InP quantum-well SCOWAs having confinement factors (Γ) of 0.5% and 1%. Bias current = 5 A. Submount temperature = 16 °C.

of wavelength. We observe that the gain does not change appreciably as the current is increased from 4 to 5 A and attribute this clamping to increased IVBA losses, as described above.

Noise figure spectra (Fig. 11) of the packaged SCOWA were measured using the optical-source-subtraction method [10], [46]. A low-power tunable CW laser was injected into the packaged SCOWA. The SCOWA output was attenuated and then measured using an optical spectrum analyzer. Calibration factors measured and included in the NF calculation were: the source-spontaneous-emission spectral density, the optical losses, and the polarization extinction of the SCOWA. At 1540 nm and 2-A bias, a noise figure of 4.6 dB was obtained. We attribute this very low NF of the packaged SCOWA to: 1) its low internal loss coefficient, 2) the high-coupling efficiency between the SCOWA and the input lensed fiber, and 3) low-population inversion factor ($n_{\rm sp} \sim 1$) due to low carrier heating [see (4)]. As the current is increased from 2 to 5 A, the NF increases due to a combination of increased loss due to IVBA, increased $n_{\rm sp}$ due to carrier heating, and decreased coupling efficiency at shorter wavelengths due to the presence of higher-order transverse modes [10]. At 5-A bias, the NF at 1540 nm increased to 5.5 dB, which is still the lowest that has been achieved to date for a fiber-coupled SOA. At biases less than 2 A, the inversion of the amplifier drops significantly, especially towards the shorter wavelengths, resulting in a larger noise figure. The accuracy of the optical-source-subtraction NF measurements was confirmed by independently measuring the NF using an electrical technique [10]. At 5-A bias, the agreement between the two NF measurement techniques was better than 0.1 dB over the tested wavelength range (1460–1580 nm).

Initial optical communication system tests were performed using an early-generation packaged SCOWA that incorporated butt-coupled, angle-cleaved SMF-28 fibers [47]. In these experiments, we compared the performance of the SCOWA power amplifier and a high-power commercial EDFA. The results of these measurements showed that the SCOWA did not introduce any receiver power-penalty relative to the EDFA for several modulation formats (binary PPM, OOK, DPSK) at bit rates above 1 Gb/s. However, for amplitude-modulated signal formats with data rates less than 1 Gb/s, the SCOWA output pulses became distorted and the transmitter efficiency decreased due to the short upper-state lifetime ($\sim$250 ps) of the quantum-well gain medium. The measured noise-figure of this early SCOWA (9 dB) was degraded by an input coupling loss of 4 dB between the SCOWA and the angle-cleaved SMF-28 fiber. This loss has been reduced to 0.5 dB by using lensed fibers as described above.

Fig. 12 shows the gain saturation characteristics of two packaged SCOWAs with nearly identical design parameters (5 InGaAsP QWs, 25-nm p-InAlAs blocking layer, 5-μm-thick waveguide, 10-mm length). The primary difference for the two SCOWAs is the value of Γ, estimated to be 0.5% and 1%, which results in G_0 of 14 and 30 dB, and $P_{o,\rm sat}$ of 0.8 and 0.4 W, respectively, at a bias current of 5 A. We note that the $G\bullet P$ product is approximately constant (11–12 W-dB) for the two SCOWAs

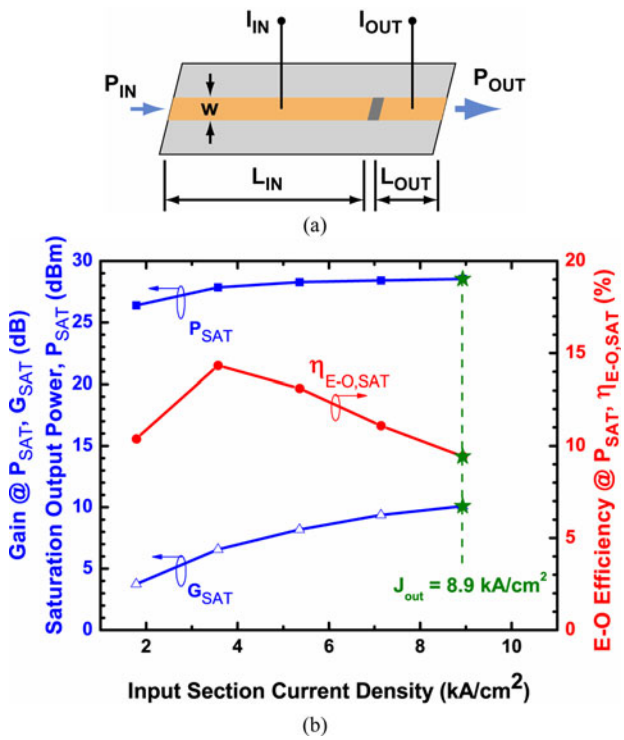

Fig. 13. Multicontact SCOWA concept and performance: (a) top view of a multicontact SCOWA showing isolated input and output sections, and (b) fiber-to-free-space output power, gain, and efficiency at the saturation output power versus the input-section current density. Fixed output-section current density $J_{\mathrm{out}} = 8.9\,\mathrm{kA/cm}^2$. Section lengths: $L_{\mathrm{IN}} = 7.5$ mm, $L_{\mathrm{OUT}} = 2.5$ mm.

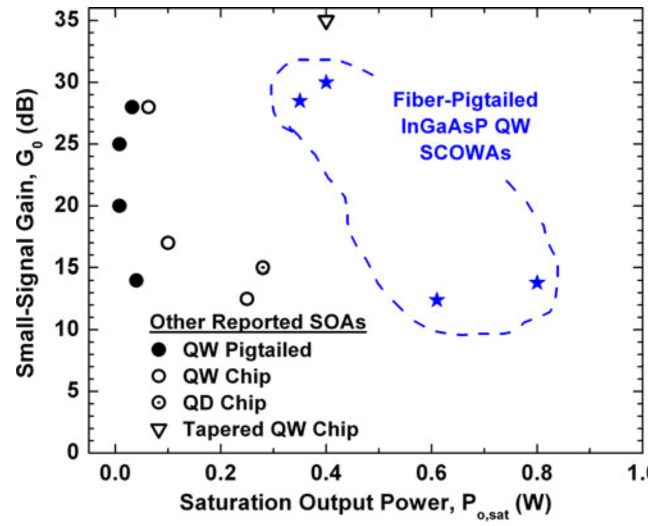

Fig. 14. Comparison of the small-signal gain versus saturation output power performance of 1.5-μm SOAs, including: pigtailed QW SCOWAs (stars), pigtailed QW SOAs (closed circles), QW chips (open circles), QD chips (dotted circle), and tapered QW chip (inverted triangle).

as is expected for SOA structures differing only in Γ [see (5)]. The saturated gain of the high-Γ SCOWA is 20 dB at 0.5-W output power, implying a required input power of only 5 mW. At 5-A bias, the maximum electrical-to-optical conversion efficiency for the low-Γ and high-Γ packaged SCOWAs is 11% and 8%, respectively.

One technique that has been demonstrated to increase the SCOWA electrical-to-optical conversion efficiency is to independently bias multiple sections of the SCOWA along its length [Fig. 13(a)] [48]. The efficacy of this multicontact technique depends on the manner in which the material gain saturates as a function of current density. To achieve large $P_{o,\mathrm{sat}}$, the gain medium must be driven deep into saturation where the differential gain $a = dg/dn$ is small [see (2)]. Therefore, the output of an SOA needs to be operated at high current density to achieve strong saturation. However, the input of an SOA needs only enough current to provide optical gain. By separating the bias electrode of an SOA into two sections, different current densities can be applied to the input and output sections.

Fig. 13(b) shows data that demonstrate the use of the multicontact technique to increase the $\eta_{e\text{-}o}$ of a SCOWA. For this demonstration, electrical isolation between the input ($L_{\mathrm{IN}} = 7.5$ mm) and output ($L_{\mathrm{OUT}} = 2.5$ mm) sections of the contact was obtained by wet etching both the p^+-InGaAs cap and metal contact. Separate diode drivers were used to supply constant current to each contact and separate sense probes were used to accurately measure the bias voltage of each section. The width of the waveguide ridge was $w = 5.8$ μm. A constant current of 1.25 A was injected into the output section, corresponding to a current density of $J_{\mathrm{OUT}} = 8.9\,\mathrm{kA/cm}^2$. Fiber-to-free-space gain-saturation characteristics (gain versus input optical power) were then measured at several input-section bias current densities J_{IN}. The measured gain-saturation characteristics were then used to determine $P_{o,\mathrm{sat}}$, the gain at saturation $G_{\mathrm{sat}} = G_0$ – 3 dB, and the efficiency at saturation $\eta_{e\text{-}o,\mathrm{sat}}$. The data in Fig. 13(b) show that maximum $P_{o,\mathrm{sat}} = 28.5$ dBm (0.7 W) and $G_{\mathrm{sat}} = 10.1$ dB both occur when $J_{\mathrm{IN}} = J_{\mathrm{OUT}}$. At this input bias, $\eta_{e\text{-}o,\mathrm{sat}} = 9.4\%$. As J_{IN} decreases, $\eta_{e\text{-}o,\mathrm{sat}}$ increases to a maximum of 14.3% at $J_{\mathrm{IN}} = 3.6\,\mathrm{kA/cm}^2$. For this same decrease in J_{IN}, $P_{o,\mathrm{sat}}$ and G_{sat} decrease by 0.6 dB and 3.5 dB, respectively. This tradeoff between increasing $\eta_{e\text{-}o,\mathrm{sat}}$ and decreasing $P_{o,\mathrm{sat}}$ and G_{sat} depends on how the gain saturates as a function of current density. As described above, the SCOWA efficiency at high-current density (e.g., $J_{\mathrm{OUT}} = 8.9\,\mathrm{kA/cm}^2$) is limited by increased nonradiative recombination, and increased optical losses due to carrier-related FCA and intensity-related TPA.

The improvement in $P_{o,\mathrm{sat}}$ of *pigtailed* 1.5-μm SCOWAs relative to other reported 1.5-μm pigtailed SOAs and SOA chips is summarized in Fig. 14 [23], [24], [34], [49]–[53]. All of the SCOWAs contained InGaAsP QWs and had a length of 10 mm. The maximum reported $P_{o,\mathrm{sat}}$ of fixed-waveguide-width QW pigtailed SOAs and SOA chips is 0.04 and 0.25 W [23], respectively. A QD SOA chip having $P_{o,\mathrm{sat}} = 0.28$ W has been reported [34]. The use of a tapered-output ($w \sim 200$ μm) SOA allows both large $P_{o,\mathrm{sat}} = 0.4$ W and large $G_0 = 35$ dB to be achieved simultaneously [49]. The pigtailed SCOWAs used both high-Γ ($\sim$1%) and low-Γ ($\sim$0.5%) designs. The $P_{o,\mathrm{sat}}$ of the high-Γ and low-Γ SCOWAs were in the range of 0.35–0.4 W and 0.6–0.8 W, respectively.

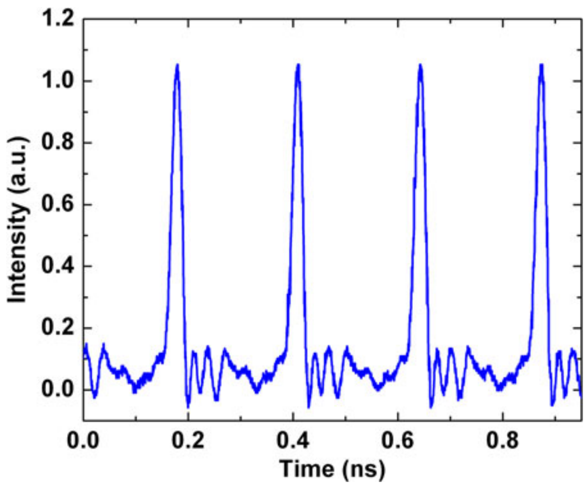

Fig. 15. Sampling-scope trace of detected pulse train generated by a 1.5-μm monolithic passively mode-locked SCOWL. Gain-bias current = 3 A. Absorber reverse-bias voltage = 1.8 V.

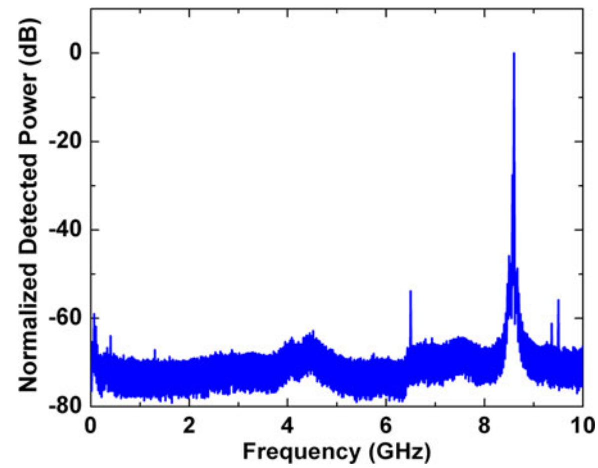

Fig. 16. Detected RF spectrum of a 1.5-μm CPM-SCOWL. Gain-bias current = 5 A. Absorber bias = 1.5 V.

III. Mode-Locked SCOW Lasers (ML-SCOWLs)

A. *Monolithic Passively ML-SCOWLs*

Passively mode-locked SCOWLs have been realized by dividing the waveguide into gain and saturable absorber sections using a multicontact electrode similar to that described above [54], [55]. The gain and absorber lengths were 9.5 and 0.5 mm, respectively. The isolation between sections was enhanced by using proton implantation in addition to etching the p^+ InGaAs cap layer and the metal contact. Dielectric coatings were evaporated on the facets to achieve 95% reflectivity on the facet adjacent to the absorber and 5% reflectivity on the output facet. The laser was mounted junction side up on a CuW submount with AuSn solder.

Passive mode-locking was achieved by injecting current into the gain section and applying a reverse bias voltage to the absorber section. At a 3-A gain-section current and 1.8-V absorber-section reverse bias, the laser produced a train of 10-ps pulses at a repetition rate of 4.3 GHz (Fig. 15). The pulse width was determined using an autocorrelator and assuming a Gaussian pulse shape. The average power was 0.25 W, implying that the peak power and pulse energy were 5.8 W and 58 pJ, respectively. To our knowledge, this demonstration represented a 10$\times$ increase in average power and a 100$\times$ increase in pulse energy relative to previously demonstrated semiconductor mode-locked lasers operating in the 1.5-μm wavelength region. Since our first demonstration another group has reported both passive and hybrid mode-locking of a monolithic SCOWL cavity with comparable output power and pulse energy [56], [57].

The optical spectrum was centered at 1544 nm and had a 3-dB bandwidth of 5.7 nm, implying a time-bandwidth product of 7.5. Temporal pulse compression was performed using lengths of SMF-28 fiber and the shortest pulse width obtained was 4 ps. This implies that the pulses contain nonlinear frequency chirp that inhibits further compression. It is likely a major contributor to the nonlinear chirp is the transient index change associated with the TPA-generated carriers that are created by the high-peak intensities of the optical pulses [44], [58]. TPA also limits the pulse energy and peak power of the optical pulses.

B. *Monolithic Colliding-Pulse Mode-Locked (CPM) SCOWLs*

The simplest way to increase the repetition rate of a passively mode-locked laser is to reduce the laser's cavity length. However, for high-power monolithic semiconductor mode-locked lasers, it is advantageous to have a long cavity to facilitate the removal of heat. We have also observed that a minimum length of about 4 mm is required to maintain single-transverse-mode operation in InGaAsP/InP SCOWLs of the present design [30].

Another method to increase the repetition rate of a monolithic passively mode-locked semiconductor laser is to use a colliding-pulse mode-locking (CPM) geometry [59]. In a CPM laser, the absorber section or sections are placed inside the cavity instead of on one end of the cavity. Appropriate choice of the absorber position creates a condition where it is favorable to have multiple pulses propagating in the cavity. By positioning the absorber in the center of the cavity [Fig. 1(b)], the laser mode-locks at twice the fundamental cavity rate so that 2 pulses counter-propagate in the cavity and collide in the absorber section.

We have realized a second-harmonic CPM-SCOWL by positioning a 0.5-mm-long absorber section in the center of a SCOWL cavity having a total length of 10 mm [60]. The gain and saturable absorber sections were electrically isolated using the same approach as described above (see Section III-A). The facets were not coated so the facet reflectivities were both about 28%. The laser was mounted junction side up on a CuW submount with AuSn solder.

By injecting current into both gain sections and applying a reverse bias to the absorber section, the CPM-SCOWL generated pulses at a repetition rate of 8.6 GHz, which is twice the rate obtained from a 10-mm-long SCOWL operated at the 4.3-GHz fundamental cavity rate (see above). The RF spectrum of the detected CPM-SCOWL pulse train (Fig. 16) shows a strong component at the 8.6-GHz second-harmonic frequency

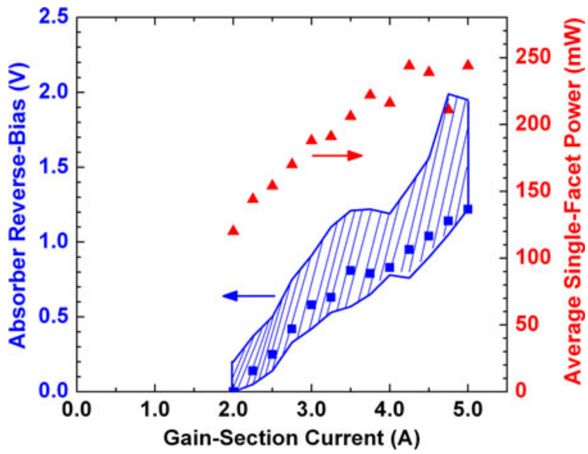

Fig. 17. Gain-section bias current and absorber-section bias voltage conditions (shaded area) for achieving mode-locked operation in a CPM-SCOWL. Average single-facet output power (triangles) and corresponding bias conditions (squares) also shown.

with more than 60-dB suppression of the 4.3-GHz fundamental frequency component. This suppression implies that both the energy and shape of the counter-propagating pulses are highly correlated.

Fig. 17 summarizes the current and voltage bias conditions over which CPM operation was achieved. The bias current was split between the two gain sections by electrically connecting the contacts in parallel. In general, the required reverse-bias voltage applied to the saturable absorber increases as the gain bias-current increases. A maximum average mode-locked output power of 0.24 W per facet was achieved at a bias current of 5 A and an absorber voltage of 1.2 V. At this bias condition, the measured pulse width was 11 ps and the time-bandwidth product was about 10, indicating that the pulses are again highly chirped.

The impact of the bias conditions on the pulse width, pulse energy, and time-bandwidth product were also investigated. Pulse widths ranging from 8 to 14 ps were obtained over the bias conditions explored. At a fixed bias current, the pulse width decreases with increasing reverse bias voltage. Increasing the reverse bias also caused the pulse energy to decrease at a fixed bias current. Pulse energies ranging from 22 to 28 pJ were obtained. The time-bandwidth product increased from 4 to 14 as the peak power of the pulses increased.

C. External-Cavity Fiber-Ring Actively ML-SCOWLs

In addition to monolithic passively mode-locked SCOWLs and CPM-SCOWLs, external-cavity actively mode-locked SCOWLs have been realized by incorporating packaged SCOWAs into fiber-ring cavities developed at the University of Central Florida [61]–[64]. The use of a long external-cavity reduces the phase noise and timing jitter of a mode-locked laser by increasing the quality factor (Q) of the cavity [65]. However, when external-cavity lasers are harmonically mode-locked to achieve high repetition rates, additional cavity components are often required to suppress supermode noise. Fig. 18 shows a fiber-ring cavity containing a lensed-fiber pigtailed SCOWA

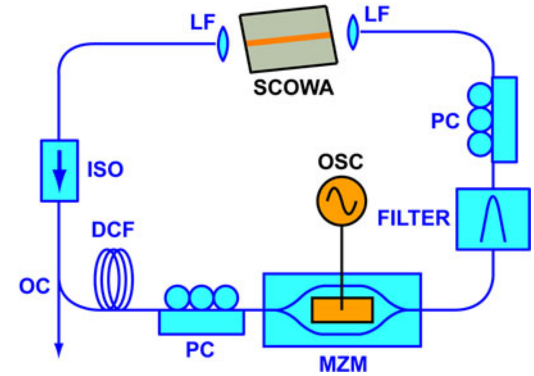

Fig. 18. Low-noise SCOWA-based fiber-ring external-cavity actively mode-locked laser. Cavity components: MZM = Mach-Zehnder modulator, OSC = microwave oscillator, FILTER = optical filter, PC = polarization controller, ISO = optical isolator, OC = output coupler, DCF = dispersion compensating fiber, and LF = lensed fiber.

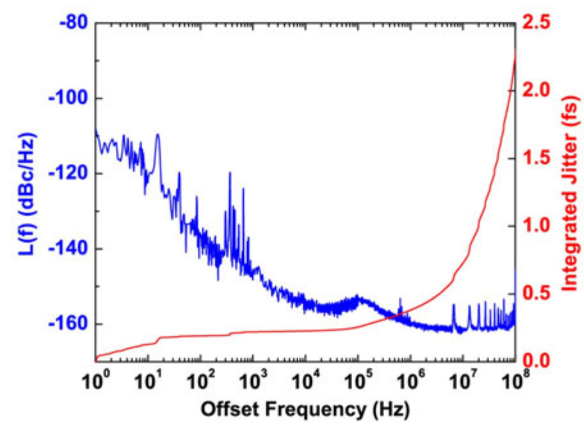

Fig. 19. Measured single-sideband residual phase-noise spectrum and corresponding integrated timing jitter of a SCOWA-based fiber-ring actively mode-locked laser.

gain medium, a $LiNbO_3$ Mach-Zehnder modulator (MZM) mode-locking element, an optical filter, a length of dispersion compensating fiber (DCF), an optical isolator, a 10% output coupler, and two polarization controllers [63]. The MZM is driven by a 10.24-GHz ultralow-noise Poseidon oscillator. The fundamental cavity frequency is ~8 MHz.

At a SCOWA bias of 4 A, the harmonically mode-locked laser produced a train of 27-ps pulses at a 10.24-GHz repetition rate. The average output power was 0.05 W implying an intracavity power of 0.5 W after the SCOWA. Fig. 19 shows the measured single-sideband residual phase-noise spectrum, revealing a corner frequency of 100 kHz and relatively small supermode power levels (~155 dBc/Hz) without any intentional supermode suppression techniques. The residual timing jitter integrated from 1 Hz to 1 MHz is 0.38 fs. To our knowledge, this is the lowest residual timing jitter reported to date from an actively mode-locked laser. A conservative estimate of the residual timing jitter integrated from 1 Hz to the Nyquist frequency (5.12 GHz) is only 7.3 fs. These results reveal the low noise and high power that can be obtained from SCOWA-based external-cavity actively mode-locked lasers.

IV. SCOW External-Cavity Lasers (SCOWECLs)

Single-frequency slab-coupled optical waveguide external-cavity lasers [SCOWECLs, see Fig. 1(c)] have been realized by combining double-pass, curved-channel (CC) SCOWAs with narrow-bandwidth fiber Bragg gratings (FBGs) [66]–[68]. The coupling between the CC-SCOWA and FBG was performed using either an angle-cleaved fiber or a lensed fiber. An optical isolator having 60-dB isolation was spliced after the FBG to minimize backreflections into the cavity.

The active section of the demonstrated SCOWECLs consisted of a 10-mm-long CC-SCOWA. The QW active region contained four 7-nm-thick compressively strained (1%) InGaAlAs wells with tensile-strained (0.3%) InGaAlAs barrier and bounding layers, and a 15-nm p-InAlAs blocking layer. The Γ of the CC-SCOWA estimated to be about 0.25%. A curved-channel waveguide geometry was used to provide both a high-reflectivity flat facet and a low-reflectivity 5°-angled facet. Due to the very low transverse index contrast ($\Delta n/n = 7 \times 10^{-4}$) of the CC-SCOWA, a large radius of curvature (R = 100 mm) was used to minimize the waveguide bend loss. The bend loss for this curved waveguide was estimated to be less than 0.1 dB. After depositing appropriate facet coatings, the estimated reflectivity of the flat and angled facets was $R > 95\%$ and $R < 10^{-5}$, respectively. The SCOWA was mounted junction-side down to a Cu-W heatsink and temperature controlled using a thermo-electric cooler.

The first demonstration of a SCOWECL used a FBG written in Flexcore 1060 fiber and having a center wavelength of 1556 nm, a FWHM bandwidth of 50 pm (6.2 GHz), and a reflectivity of R = 50% [66]. The mode diameter of the Flexcore 1060 fiber is 6.5 μm, making it well matched to the SCOWA mode. The FBG was cleaved near one end of the grating at an 11° angle to allow maximum coupling when the SCOWA and FBG facets are parallel. The CC-SCOWA and FBG were then aligned, butt-coupled, and fixed in position using a laser-welded fiber-pigtailed assembly process. The 2-A threshold current of the pigtailed SCOWECL was much larger than the 1-A threshold obtained on the bench, indicating a coupling misalignment during packaging. This initial SCOWECL achieved stable single-longitudinal-mode operation for only several small current windows ($\Delta I \sim 20$ mA) spaced between I = 2.5 and 3.5 A. The line shape was measured to have a Voigt distribution using the self-heterodyne linewidth measurement technique with a differential delay of 250 μs. The Voigt line shape has a Lorentzian (white noise) tail that is spectrally broadened by 1/f noise to produce a Gaussian central component. At an output power of 88 mW (I = 3.18 A), the Gaussian FWHM linewidth was estimated to be $\Delta\nu = 130$ kHz.

Several modifications were made to the SCOWECL cavity to dramatically improve its performance [67], [68]: 1) reduced the number of longitudinal modes within the FBG reflection band by decreasing the FWHM bandwidth of the FBG from 50 to 20 pm, 2) decreased the FBG reflectivity from 50% to 20% to increase the output power, 3) increased the SCOWA-to-FBG coupling efficiency by using a lensed fiber (6.5-μm spot size) instead of an angle-cleaved fiber, and 4) reduced the linewidth enhancement factor by red-shifting the bandgap wavelength of the QW active region from 1530 to 1565 nm so that the 1550-nm lasing wavelength set by the FBG was on the short-wavelength ("blue") side of the SCOWA gain peak. The lensed fiber and FBG were fusion spliced to create the passive section of the external-cavity laser. Care was taken to minimize the length of the lensed-fiber section to minimize the free spectral range (FSR) of the laser cavity. The lensed fiber was cleaved to a length of ~3 cm, which is the minimum length necessary for handling in our fusion splicer. Prior to splicing, an optical backscatter reflectometer was used to identify the beginning of the FBG index profile so that excess fiber could be removed from the FBG as well.

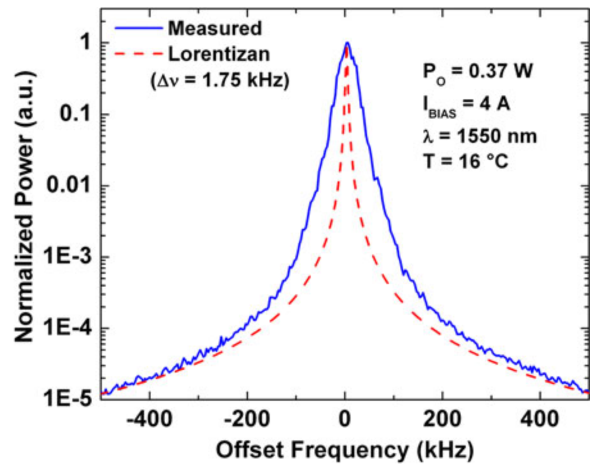

Fig. 20. Line shape of a packaged SCOWECL at 4-A bias current. Laser output power = 0.37 W. Lorentzian line shape ($\Delta\nu_L = 1.75$ kHz) also shown (dashed).

The threshold current of the modified SCOWECL was 0.9 A and a maximum output power of 0.37 W was attained at I = 4 A [67]. The laser exhibited much better single-longitudinal-mode stability than the initial version for bias current I < 4 A. The power-current (L-I) curve (not shown) exhibited a jagged characteristic due to longitudinal-mode hopping. The electrical-to-optical conversion efficiency at 4 A was calculated to be $\eta_{e\text{-}o} = 7\%$. The observed rollover in the L-I characteristic is attributed primarily to increased optical losses associated with TPA as described above. Before deciding to use a FBG having R = 20%, we determined that higher output power could be obtained with R = 10% ($P_O = 0.46$ W at I = 4 A) at the expense of degraded laser noise performance [68].

The spectral lineshape of the modified SCOWECL at I = 4 A (Fig. 20) was determined to have a Voigt distribution by using the self-heterodyne measurement technique. The Gaussian FWHM linewidth was $\Delta\nu_G = 35$ kHz and the Lorentzian linewidth was $\Delta\nu_L \sim 1.75$ kHz. To our knowledge, this is the smallest Lorentzian linewidth from a semiconductor laser having $P_o >$ 0.1 W.

The measured relative intensity noise (RIN) spectrum of the modified SCOWECL at I = 4 A (Fig. 21) was shot-noise limited ($I_{PD} = 5$ mA) at −162 dB/Hz from 0.2 to 10 GHz. The RIN was measured using a 40-GHz photodiode, high-gain amplifier, and

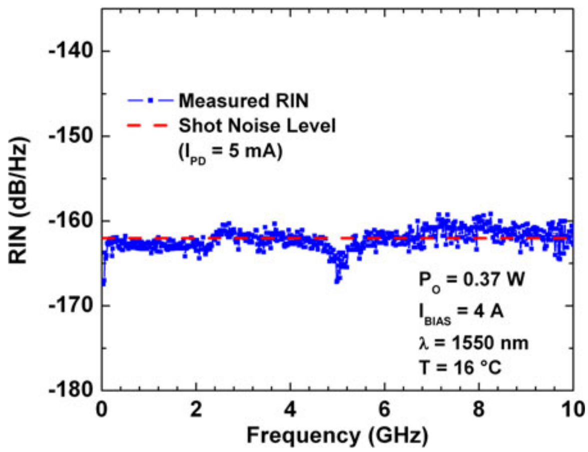

Fig. 21. Relative intensity noise (RIN) spectrum of a packaged SCOWECL at 4-A bias current. Laser output power = 0.37 W. Shot-noise limited RIN of photodiode also shown (dashed).

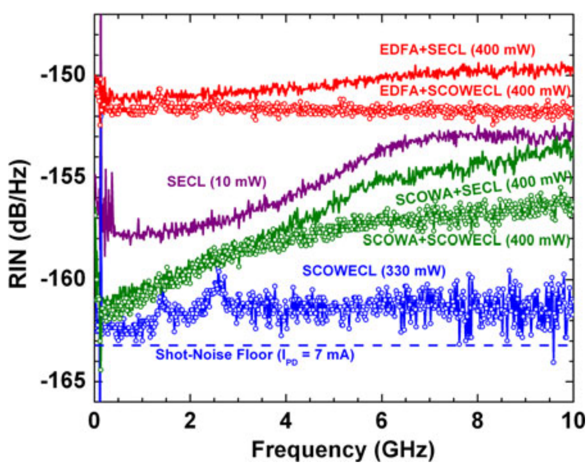

Fig. 22. Relative intensity noise (RIN) spectra of SCOWECL and commercial SECL: (a) without amplification, (b) amplified by a SCOWA, and (c) amplified by a high-power EDFA. Fixed detected photocurrent = 7 mA.

electronic spectrum analyzer. Note that there is no evidence of either a relaxation oscillation resonance or residual sidemodes above the shot-noise floor. This implies that the sidemode suppression ratio (SMSR) exceeds 80 dB. Calculations predict that the relaxation oscillation should be below this shot-noise level for the SCOWA gain medium and cavity used here.

We also measured the RIN spectra of a second modified, packaged SCOWECL and compared it to that of a commercial semiconductor external-cavity laser (SECL) under both unamplified and amplified conditions (Fig. 22). The unamplified SCOWECL and SECL output powers were 330 and 10 mW, respectively. Two amplifiers were compared: 1) the packaged high-Γ SCOWA characterized in Fig. 12, and 2) a commercial 2-W EDFA with a specified NF of 5 dB. For the MOPA-configuration measurements, the amplifier input power was fixed at 10 mW by using the direct SECL output or the attenuated output of the SCOWECL operating at 330-mW output power. The amplifier gains were then adjusted to obtain 400-mW output power. In all cases, the optical signals were attenuated to obtain a fixed photocurrent of 7 mA, which is below the saturation current of the photodiode used.

The data of Fig. 22 reveal that the RIN of the unamplified SCOWECL is smaller than that of the SECL or either of the MOPA configurations. The SCOWECL RIN is approximately equal to the shot-noise level (∼163 dB/Hz) with no visible relaxation oscillation. The SECL RIN is 5-dB above the shot-noise floor at low frequencies and shows evidence of a relaxation oscillation in the 7–10 GHz region. The EDFA RIN is at least 10 dB larger than the SCOWECL RIN for similar output powers. The SCOWA RIN is lower than the EDFA RIN and exhibits RIN suppression at low frequencies as has been observed previously in saturated SOAs [69]. We note that the commercial high-power EDFA tested here was not optimized for low RIN or low NF. It is possible that lower EDFA noise can be obtained through appropriate design.

V. Discussion

The SCOW geometry has enabled the realization of a variety of high-power semiconductor optical amplifiers and lasers. Using the InP quantum-well material system at an optical wavelength 1.5-μm, we have demonstrated fiber-pigtailed power amplifiers (SCOWAs) having saturation output power ranging from 0.4 to 0.8 W, monolithic mode-locked lasers (ML-SCOWLs) operating at 4.3- and 8.6-GHz rates and producing 100s of milliwatts average output power, external-cavity mode-locked lasers having <10 fs residual timing jitter, and high-power, single-frequency external-cavity lasers (SCOWECLs) with narrow linewidth and low RIN. The SCOWA is a strong candidate for the replacement of Watt-class EDFAs for some applications because of its relatively small size, wide optical bandwidth, and high electrical-to-optical conversion efficiency. The reported low-noise figure of the SCOWA is also comparable to that of conventional Watt-class EDFAs. Although beyond the scope of this paper, we also note that the large-mode, low-Γ attributes of the SCOW geometry are also beneficial to the realization of high-current waveguide photodiodes [70].

The output power and conversion efficiency of InP-based SCOWAs are limited by the optical losses associated with TPA and TPA-generated FCA in the InGaAsP waveguide where the mode intensity is largest. These TPA-induced limits are observed more readily in SCOWA structures than in conventional SOAs because of the larger impact of the internal loss coefficient (α_i) on low-Γ gain media. However, it is likely that TPA-generated FCA has limited the CW gain and output power of previously reported SOAs and semiconductor lasers, especially those having small Γ. Our results also provide evidence that nonlinear gain compression, which describes the reduction in material gain at high optical intensity, is partially due to TPA. The large mode size of the SCOWA (∼5.5 × 7.5 μm) acts to reduce the transverse mode intensity and enables a maximum output power on the order of 1 W.

Several techniques may be applied to mitigate the effect of TPA on the output power of low-Γ SOAs and lasers. First, the size of the optical mode could be increased to decrease the optical intensity, thereby decreasing α_2. Second, the waveguide could be designed from a material having a bandgap energy that is at least twice the photon energy so that TPA would be effectively eliminated. Third, non-radiative recombination centers could be introduced into the waveguide through low-temperature growth or proton bombardment. These recombination centers would reduce the lifetime τ_2 of the TPA-generated carriers, thereby decreasing the associated FCA [see (8)]. And fourth, the waveguide could be designed so that the peak of the optical mode was in the high-field region of a p-i-n diode. Sweepout of the TPA-generated carriers would again reduce τ_2.

In addition to mitigating the TPA-induced limits, the SCOWA gain medium will likely benefit from additional design improvements including variable-confinement and the use of QD active regions. In a fixed-Γ SOA, a tradeoff exists between gain and output power (see Fig. 12). To simultaneously obtain high gain and high output power, Γ can be varied along the length of the waveguide. In a variable-Γ SOA, the input section has high Γ (large G_0, small $P_{o,\text{sat}}$) and the output section has low Γ (small G_0, large $P_{o,\text{sat}}$). Although all of our SCOWA work to date has involved the use of QW active regions, it is possible that increased $P_{o,\text{sat}}$ may be obtained using a QD active region due to the small differential gain at high-injection current [36]. Other benefits of the use of QDs in SOAs relative to QWs include increased gain bandwidth, and ultrafast gain recovery to minimize patterning effects in optical communication systems [35].

Acknowledgment

The authors thank F. Quinlan, D. Mandridis, and S. Ozharar of the University of Central Florida for development of the SCOWA-based fiber-ring mode-locked lasers. The authors recognize the technical contributions of R. K. Huang and B. Chann of Teradiode, Inc. in the development of the SCOWLs and passively mode-locked SCOWLs. The authors also acknowledge valuable discussions with A. K. Goyal, D. O. Caplan, S. A. Hamilton, J. C. Twichell, and G. W. Turner of Lincoln Laboratory; A. R. Motamedi, R. J. Ram, and Prof. E. P. Ippen of MIT; and D. Sparacin of Booz Allen Hamilton. The authors are also very thankful for the support and guidance of S. A. Pappert and R. D. Esman of the Defense Advanced Projects Agency (DARPA).

References

[1] Y. Jeong, J. K. Sahu, D. B. S. Soh, C. A. Codemard, and J. Nilsson, “High-power tunable single-frequency single-mode erbium:ytterbium codoped large-core fiber master-oscillator power amplifier source,” *Opt. Lett.*, vol. 30, no. 22, pp. 2997–2999, 2005.

[2] “EAR-LP Series Linearly Polarized Erbium-Doped Fiber Amplifier Specifications,” IPG Photonics Corp. Website, 2010.

[3] D. J. Jones, S. A. Diddams, J. K. R. Ranka, A. Stentz, R. S. Windeler, J. L. Hall, and S. T. Cundiff, “Carrier-envelope phase control of femtosecond mode-locked lasers and direct optical frequency synthesis,” *Science*, vol. 288, no. 5466, pp. 635–639, 2000.

[4] S. A. Diddams, A. Bartels, T. M. Ramond, C. W. Oates, S. Bize, E. A. Curtis, J. C. Bergquist, and L. Hollberg, “Design and control of femtosecond lasers for optical clocks and the synthesis of low-noise optical and microwave signals,” *IEEE J. Sel. Top. Quantum Electron.*, vol. 9, no. 4, pp. 1072–1080, Jul./Aug. 2003.

[5] B. R. Washburn, S. A. Diddams, N. R. Newbury, J. W. Nicholson, M. F. Yan, and C. G. Jrgensen, “Phase-locked, erbium-fiber-laser-based frequency comb in the near infrared,” *Opt. Lett.*, vol. 29, no. 3, pp. 250–252, 2004.

[6] C. Henry, “Theory of the linewidth of semiconductor lasers,” *IEEE J. Quantum Electron.*, vol. 18, no. 2, pp. 259–264, Feb. 1982.

[7] P. W. Juodawlkis, J. J. Plant, R. K. Huang, L. J. Missaggia, and J. P. Donnelly, “High-power 1.5-μm InGaAsP/InP slab-coupled optical waveguide amplifier,” *IEEE Photon. Technol. Lett.*, vol. 17, no. 2, pp. 279–281, Feb. 2005.

[8] P. W. Juodawlkis, J. J. Plant, W. Loh, L. J. Missaggia, K. E. Jensen, and F. J. O’Donnell, “Packaged 1.5-μm quantum-well SOA with 0.8-W output power and 5.5-dB noise figure,” *IEEE Photon. Technol. Lett.*, vol. 21, no. 17, pp. 1208–1210, Sep. 2009.

[9] G. P. Agrawal and N. K. Dutta, *Semiconductor Lasers*, 2nd ed. New York: Van Nostrand Reinhold, 1993.

[10] W. Loh, J. J. Plant, J. Klamkin, J. P. Donnelly, F. J. O’Donnell, R. J. Ram, and P. W. Juodawlkis, “Noise figure of Watt-class ultralow-confinement semiconductor optical amplifiers,” *IEEE J. Quantum Electron.*, vol. 47, no. 1, pp. 66–75, Jan. 2011.

[11] J. Simon, “GaInAsP semiconductor laser amplifiers for single-mode fiber communications,” *J. Lightw. Technol.*, vol. 5, no. 9, pp. 1286–1295, 1987.

[12] M. J. O’Mahony, “Semiconductor laser optical amplifiers for use in future fiber systems,” *J. Lightw. Technol.*, vol. 6, no. 4, pp. 531–544, 1988.

[13] N. A. Olsson, “Semiconductor optical amplifiers,” *Proc. IEEE*, vol. 80, no. 3, pp. 375–382, 1992.

[14] M. J. Connelly, *Semiconductor Optical Amplifiers*. New York: Springer, 2002.

[15] J. E. Bowers, “High speed semiconductor laser design and performance,” *Solid-State Electron.*, vol. 30, no. 1, pp. 1–11, 1987.

[16] J. N. Walpole, E. S. Kintzer, S. R. Chinn, C. A. Wang, and L. J. Missaggia, “High-power strained-layer InGaAs/AlGaAs tapered traveling wave amplifier,” *Appl. Phys. Lett.*, vol. 61, no. 7, pp. 740–742, 1992.

[17] D. Mehuys, D. F. Welch, and L. Goldberg, “2.0 W CW, diffraction-limited tapered amplifier with diode injection,” *Electron. Lett.*, vol. 28, no. 21, pp. 1944–1946, 1992.

[18] F. Koyama, K.-Y. Liou, A. G. Dentai, T. Tanbun-ek, and C. A. Burrus, “Multiple-quantum-well GaInAs/GaInAsP tapered broad-area amplifiers with monolithically integrated waveguide lens for high-power applications,” *IEEE Photon. Technol. Lett.*, vol. 5, no. 8, pp. 916–919, Aug. 1993.

[19] J. P. Donnelly, J. N. Walpole, G. E. Betts, S. H. Groves, J. D. Woodhouse, F. J. O’Donnell, L. J. Missaggia, R. J. Bailey, and A. Napoleone, “High-power 1.3-μm InGaAsP-InP amplifiers with tapered gain regions,” *IEEE Photon. Technol. Lett.*, vol. 8, no. 11, pp. 1450–1452, Nov. 1996.

[20] I. B. Petrescu-Prahova, M. Buda, and T. G. van de Roer, “Design of a 1 W, single filament laser diode,” *IEICE Trans. Electron.*, vol. E77-C, no. 9, pp. 1472–1478, 1994.

[21] L. J. Mawst, A. Bhattacharya, J. Lopez, D. Botez, D. Z. Garbuzov, L. DeMarco, J. C. Connolly, M. Jansen, F. Fang, and R. F. Nabiev, “8 W continuous wave front-facet power from broad-waveguide Al-free 980 nm diode lasers,” *Appl. Phys. Lett.*, vol. 69, no. 11, pp. 1532–1534, 1996.

[22] D. Garbuzov, L. Xu, S. R. Forrest, R. Menna, R. Martinelli, and J. Connolly, “1.5-μm wavelength, SCH-MQW InGaAsP/InP broadened-waveguide laser diodes with low internal loss and high output power,” *Electron. Lett.*, vol. 32, no. 18, pp. 1717–1718, 1996.

[23] K. Morito, S. Tanaka, S. Tomabechi, and A. Kuramata, “A broad-band MQW semiconductor optical amplifier with high saturation output power and low noise figure,” *IEEE Photon. Technol. Lett.*, vol. 17, no. 5, pp. 974–976, May 2005.

[24] M. Dagenais, P. Heim, S. Saini, S. Wilson, R. Leavitt, A. Yu, T. Horton, V. Luciani, D. Stone, and Y. Hu, “High-power C-band semiconductor booster optical amplifier,” in *Proc. Opt. Fiber Commun. (OFC) Conf.*, Mar., 2003, pp. 85–87.

[25] J. W. Raring, E. J. Skogen, M. L. Masanovic, S. P. DenBaars, and L. A. Coldren, “Demonstration of high saturation power/high gain SOAs using quantum well intermixing based integration platform,” *Electron. Lett.*, vol. 41, no. 24, pp. 1345–1346, 2005.

[26] E. A. J. Marcatili, “Slab-coupled waveguides,” *Bell Syst. Tech. J.*, vol. 53, pp. 645–672, 1974.

[27] J. N. Walpole, J. P. Donnelly, P. J. Taylor, L. J. Missaggia, C. T. Harris, R. J. Bailey, A. Napoleone, S. H. Groves, S. R. Chinn, R. K. Huang, and J. J. Plant, “Slab-coupled 1.3-μm semiconductor laser with single-spatial, large-diameter, single-lobed mode,” *IEEE Photon. Technol. Lett.*, vol. 14, no. 6, pp. 756–758, Jun. 2002.

[28] J. P. Donnelly, R. K. Huang, J. N. Walpole, L. J. Missaggia, C. T. Harris, J. J. Plant, R. J. Bailey, D. E. Mull, W. D. Goodhue, and G. W. Turner, "AlGaAs-InGaAs slab-coupled optical waveguide lasers," *IEEE J. Quantum Electron.*, vol. 39, no. 2, pp. 289–298, Feb. 2003.

[29] R. K. Huang, J. P. Donnelly, L. J. Missaggia, C. T. Harris, J. J. Plant, D. E. Mull, and W. D. Goodhue, "High-power nearly diffraction-limited AlGaAs-InGaAs semiconductor slab-coupled optical waveguide laser," *IEEE Photon. Technol. Lett.*, vol. 15, no. 7, pp. 900–902, Jul. 2003.

[30] J. J. Plant, P. W. Juodawlkis, R. K. Huang, J. P. Donnelly, L. J. Missaggia, and K. G. Ray, "1.5-μm InGaAsP-InP slab-coupled optical waveguide lasers," *IEEE Photon. Technol. Lett.*, vol. 17, no. 4, pp. 735–737, Apr. 2005.

[31] G. M. Smith, R. K. Huang, J. P. Donnelly, L. J. Missaggia, M. K. Connors, G. W. Turner, and P. W. Juodawlkis, "High-power slab-coupled optical waveguide lasers," in *Proc. IEEE Photon. Soc. Annu. Meet.*, Nov. 2010, pp. 479–480.

[32] P. W. Juodawlkis and J. J. Plant, "Gain-power trade-off in low-confinement semiconductor optical amplifiers," in *Proc. Int. Conf. Numerical Simul. Optoelectronic Devices (NUSOD)*, Sep. 2007, pp. 97–98.

[33] P. M. Smowton and P. Blood, "The differential efficiency of quantum-well lasers," *IEEE J. Sel. Top. Quantum Electron.*, vol. 3, no. 2, pp. 491–498, Apr. 1997.

[34] T. Akiyama, M. Ekawa, M. Sugawara, K. Kawaguchi, H. Sudo, A. Kuramata, H. Ebe, and Y. Arakawa, "An ultrawide-band semiconductor optical amplifier having an extremely high penalty-free output power of 23 dBm achieved with quantum dots," *IEEE Photon. Technol. Lett.*, vol. 17, no. 8, pp. 1614–1616, Aug. 2005.

[35] T. Akiyama, M. Sugawara, and Y. Arakawa, "Quantum-dot semiconductor optical amplifiers," *Proc. IEEE*, vol. 95, no. 9, pp. 1757–1766, 2007.

[36] T. W. Berg and J. Mork, "Saturation and noise properties of quantum-dot optical amplifiers," *IEEE J. Quantum Electron.*, vol. 40, no. 11, pp. 1527–1539, Nov. 2004.

[37] M. J. Connelly, "Wideband semiconductor optical amplifier steady-state numerical model," *IEEE J. Quantum Electron.*, vol. 37, no. 3, pp. 439–447, Mar. 2001.

[38] L. A. Coldren and S. W. Corzine, *Diode Lasers and Photonic Integrated Circuits*. New York: John Wiley & Sons, Inc, 1995.

[39] J. Minch, S. H. Park, T. Keating, and S. L. Chuang, "Theory and experiment of $In_{1-x}Ga_xAs_yP_{1-y}$ and $In_{1-x-y}Ga_xAl_yAs$ long-wavelength strained quantum-well lasers," *IEEE J. Quantum Electron.*, vol. 35, no. 5, pp. 771–782, May 1999.

[40] P. W. Juodawlkis, J. J. Plant, J. P. Donnelly, A. Motamedi, and E. P. Ippen, "Continuous-wave two-photon absorption in a Watt-class semiconductor optical amplifier," *Opt. Exp.*, vol. 16, no. 16, pp. 12387–12396, 2008.

[41] V. Mikhaelashvili, N. Tessler, R. Nagar, G. Eisenstein, A. G. Dentai, S. Chandrasakhar, and C. H. Joyner, "Temperature dependent loss and overflow effects in quantum well lasers," *IEEE Photon. Technol. Lett.*, vol. 6, no. 11, pp. 1293–1296, Nov. 1994.

[42] D. Garbuzov, G. Shiau, x, J, V. Bulovic, M. Boroditsky, C. P. Chao, and S. R. Forrest, "Photoluminescence study of excess carrier spillover in 1.3-μm wavelength strained multi-quantum-well InGaAsP/InP laser structures," *Appl. Phys. Lett.*, vol. 66, no. 11, pp. 1307–1309, 1995.

[43] A. Pietrzak *et al.*, "55 W peak power from 1100 nm wavelength 60 μm broad-area laser diodes enabled by reduced carrier accumulation in the waveguide," *Semicond. Sci. Technol.*, vol. 24, no. 3, p. 035020, 2009.

[44] A. Motamedi, J. J. Plant, J. P. Donnelly, P. W. Juodawlkis, and E. P. Ippen, "Ultrafast nonlinearities and gain dynamics in high-power semiconductor amplifiers," *Appl. Phys. Lett.*, vol. 93, no. 25, pp. 251106.1–251106.3, 2008.

[45] S. Seki, H. Oohashi, H. Sugiura, T. Hirono, and K. Yokoyama, "Study on the dominant mechanisms for the temperature sensitivity of threshold current in 1.3-μm InP-based strained-layer quantum-well lasers," *IEEE J. Quantum Electron.*, vol. 32, no. 8, pp. 1478–1486, Aug. 1996.

[46] W. Loh, J. J. Plant, F. J. O'Donnell, and P. W. Juodawlkis, "Noise figure of a packaged, high-power slab-coupled optical waveguide amplifier (SCOWA)," in *Proc. IEEE LEOS Annual Meeting*, Nov. 2008, pp. 852–853.

[47] D. O. Caplan, P. W. Juodawlkis, J. J. Plant, and M. L. Stevens, "Performance of high-sensitivity OOK, PPM, and DPSK communications using high-power slab-coupled optical waveguide amplifier (SCOWA) based transmitters" in *Proc. Opt. Fiber Commun. (OFC) Conf.*, 2006, paper OThG7.

[48] J. J. Plant, A. K. Goyal, D. C. Oakley, D. C. Chapman, A. Napoleone, and P. W. Juodawlkis, "Improving the efficiency of high-power semiconductor optical amplifiers," in *Proc. Conf. Lasers Electro-Opt. (CLEO)*, May 2008, pp. 1–2.

[49] G. E. Betts, J. P. Donnelly, J. N. Walpole, S. H. Groves, F. J. O'Donnell, L. J. Missaggia, R. J. Bailey, and A. Napoleone, "Semiconductor laser sources for externally modulated microwave analog links," *IEEE Trans. Microwave Theory Tech.*, vol. 45, no. 8, pp. 1280–1287, Aug. 1997.

[50] "APOAM1115 1550-nm SOA Datasheet," Axon Photonics.

[51] "Alcatel 1901 SOA Datasheet," Alcatel-Lucent.

[52] "1550 nm (C-Band) Polarization-Dependent BOA Datasheet," Thorlabs, 2010.

[53] "SOA-L-C-14-FCA – 1.55-μm Linear SOA Datasheet," CIP Technologies, 2010.

[54] J. J. Plant, J. T. Gopinath, B. Chann, D. J. Ripin, R. K. Huang, and P. W. Juodawlkis, "250-mW, 1.5-μm monolithic passively mode-locked slab-coupled optical waveguide laser," *Opt. Lett.*, vol. 31, no. 2, pp. 223–225, 2006.

[55] J. T. Gopinath, J. J. Plant, B. Chann, R. K. Huang, C. T. Harris, L. J. Missaggia, J. P. Donnelly, P. W. Juodawlkis, and D. J. Ripin, "High-power monolithic passively mode-locked slab-coupled optical waveguide lasers," in *Proc. Conf. Lasers Electro-Opt. (CLEO)*, May 2006, pp. 1–2.

[56] F. R. Ahmad and F. Rana, "Passively mode-locked high-power (210 mW) semiconductor lasers at 1.55-μm wavelength," *IEEE Photon. Technol. Lett.*, vol. 20, no. 3, pp. 190–192, Feb. 2008.

[57] F. R. Ahmad and F. Rana, "Fundamental and subharmonic hybrid mode-locking of a high-power (220 mW) monolithic semiconductor laser," *IEEE Photon. Technol. Lett.*, vol. 20, no. 15, pp. 1308–1310, Aug. 2008.

[58] F. R. Ahmad, Y. W. Tseng, M. A. Kats, and F. Rana, "Energy limits imposed by two-photon absorption for pulse amplication in high power semiconductor optical ampliers," *Opt. Lett.*, vol. 33, no. 10, pp. 1041–1043, 2008.

[59] Y.-K. Chen and M. C. Wu, "Monolithic colliding-pulse mode-locked quantum-well lasers," *IEEE J. Quantum Electron.*, vol. 28, no. 10, pp. 2176–2185, Oct. 1992.

[60] J. J. Plant and P. W. Juodawlkis, "High-power 1.5-μm InGaAsP/InP colliding-pulse mode-locked slab-coupled optical waveguide laser," in *Proc. IEEE LEOS Annu. Meet.*, Oct./Nov., 2006, pp. 794–795.

[61] S. Gee, F. Quinlan, S. Ozharar, P. J. Delfyett, J. J. Plant, and P. W. Juodawlkis, "Ultralow-noise mode-locked optical pulse trains from an external cavity laser based on a slab coupled optical waveguide amplifier (SCOWA)," *Opt. Lett.*, vol. 30, no. 20, pp. 2742–2744, 2005.

[62] S. Gee, S. Ozharar, F. Quinlan, J. J. Plant, P. W. Juodawlkis, and P. J. Delfyett, "Self-stabilization of an actively mode-locked semiconductor-based fiber-ring laser for ultralow jitter," *IEEE Photon. Technol. Lett.*, vol. 19, no. 7, pp. 498–500, Apr. 2007.

[63] S. Gee, S. Ozharar, J. J. Plant, P. W. Juodawlkis, and P. J. Delfyett, "Intracavity dispersion effect on timing jitter of ultralow noise mode-locked semiconductor based external-cavity laser," *Opt. Lett.*, vol. 34, no. 3, pp. 238–240, 2009.

[64] D. Mandridis, I. Ozdur, F. Quinlan, M. Akbulut, J. J. Plant, P. W. Juodawlkis, and P. J. Delfyett, "Low-noise, low repetition rate, semiconductor-based mode-locked laser source suitable for high bandwidth photonic analog-digital conversion," *Appl. Opt.*, vol. 49, no. 15, pp. 2850–2857, 2010.

[65] F. Quinlan, S. Ozharar, S. Gee, and P. J. Delfyett, "Harmonically mode-locked semiconductor-based lasers as high repetition rate ultralow noise pulse train and optical frequency comb sources," *J. Opt. A: Pure Appl. Opt.*, vol. 11, no. 10, p. 103001, 2009.

[66] P. W. Juodawlkis, J. J. Plant, F. J. O'Donnell, L. J. Missaggia, R. K. Huang, and J. P. Donnelly, "Narrow-linewidth, high-power 1556-nm slab-coupled optical waveguide external-cavity laser," in *Proc. Conf. Lasers Electro-Opt. (CLEO)*, May 2005, pp. 411–413.

[67] P. W. Juodawlkis, W. Loh, F. J. O'Donnell, M. A. Brattain, and J. J. Plant, "Ultralow-noise packaged 1.55-μm semiconductor external-cavity laser with 0.37-W output power," in *Proc. Conf. Lasers Electro-Opt. (CLEO)*, Jun., 2009, paper CPDA3, pp. 1–2.

[68] P. W. Juodawlkis, W. Loh, F. J. O'Donnell, M. A. Brattain, and J. J. Plant, "High-power, ultralow-noise semiconductor external cavity lasers based on low-confinement optical waveguide gain media," in *Proc. SPIE Novel In-Plane Semicond. Lasers IX*, 2010, pp. 76160-1–76160-9.

[69] T. Yamatoya, F. Koyama, and K. Iga, "Noise suppression and intensity modulation using gain-saturated semiconductor optical amplifier," in *Proc. Integr. Photon. Res. (IPR)*, 2000, pp. 72–74.

[70] S. M. Madison, J. J. Plant, D. C. Oakley, D. C. Chapman, A. Napoleone, and P. W. Juodawlkis, "Slab-coupled optical waveguide photodiode," in *Proc. Conf. Lasers Electro-Opt. (CLEO)*, May 2008, pp. 1–2.

Paul W. Juodawlkis (S'86–M'86–SM'06) received the B. S. degree from Michigan Technological University, Houghton, the M.S. degree from Purdue University, West Lafayette, IN, and the Ph.D. degree from the Georgia Institute of Technology, Atlanta, all in electrical engineering.

From 1988 to 1993, he was a Technical Staff Member at Lincoln Laboratory, Massachusetts Institute of Technology (MIT), Lexington, where he was a Hardware Systems Engineer on a multisensor airborne testbed program. He then joined the Ultrafast Optical Communications Laboratory (UFOCL), Georgia Institute of Technology. In 1999, he rejoined the Lincoln Laboratory, MIT, as a member of the Electro-Optic Materials and Devices Group. He is currently Assistant Group Leader of the Electro-Optic Materials and Devices Group at the Lincoln Laboratory, MIT, where he is leading research on semiconductor optoelectronic devices and microwave photonics. His research efforts have focused on the development of optical sampling techniques for photonic analog-to-digital converters (ADCs), quantum-well electrorefractive modulators, high-power waveguide photodiodes, and high-power semiconductor optical amplifiers (SOAs) and their application in mode-locked lasers and narrow-linewidth external-cavity lasers.

Dr. Juodawlkis was the Program Co-Chair of the 2010 Conference on Lasers and Electro-Optics (CLEO). He is currently a member of the IEEE Photonics Society Board of Governors (2011–2013). He has served as Chair of the IEEE Photonics Society Technical Committee on Microwave Photonics (2003–2006), Program Co-Chair of the 2003 Photonics Society Summer Topical Meeting on Photonic Time/Frequency Measurement and Control, and committee member of the International Topical Meeting on Microwave Photonics (2004, 2008). He is also a member of the Optical Society of America (OSA) and the American Association for the Advancement of Science (AAAS).

Jason J. Plant received the B.S. degree in physics and the M.S. degree in applied physics (optical sciences) from the University of Massachusetts Lowell, in 1999 and 2001, respectively. As an undergraduate, he interned at Raytheon Company, Andover, Massachusetts, studying GaAs-based PHEMT reliability. His graduate work focused on the development and characterization of an external-cavity actively-mode-locked semiconductor laser.

He is currently an Associate Staff Member in the Electro-Optical Materials and Devices Group at Lincoln Laboratory, Massachusetts Institute of Technology (MIT), Lexington, where he is involved in the fabrication, packaging, and characterization of advanced optoelectronic components. His efforts have included the development of monolithic semiconductor mode-locked lasers, high-power semiconductor lasers and optical amplifiers, semiconductor external-cavity lasers, hybrid silicon-III/V integration, and quantum cascade lasers (QCLs).

William Loh received the B.S. degree in electrical engineering from the University of Michigan, Ann Arbor, in 2007, and the M.S. degree in electrical engineering from the Massachusetts Institute of Technology, Cambridge, in 2009. He is currently pursing the Ph.D. degree in electrical engineering from the Massachusetts Institute of Technology, Cambridge.

His research interests include high-power semiconductor amplifiers and lasers and studies of noise processes in semiconductor optical devices.

Leo J. Missaggia received the A.S. degree in mechanical engineering technology from Franklin Institute of Boston, MA, in 1980, the B.S degree in mechanical engineering from Northeastern University, Boston, MA, in 1988, and the M.S. degree in mechanical engineering from Boston University, MA, in 1994.

He is an Associate Technical Staff Member in the Electro-Optical Materials and Devices Group at MIT Lincoln Laboratory, Lexington, MA, which he joined in 1980. He has participated in numerous research projects related to electro-optical device development, in particular the development of high-power semiconductor diode lasers (both single elements and arrays). His expertise has been in the areas of device fabrication, electro-optical characterization, and device packaging including thermal management, alignment and attachment of micro-optics, and optical fibers. He contributed to the development of the first CW, 2-watt level, diffraction-limited tapered diode laser. He was also involved in the development of high-performance micro-channel heat sinks, which were required for cooling high-power 2-D laser arrays. Over this past decade, his efforts have been in the development of advanced packaging of high power slab-coupled optical waveguide laser and amplifier arrays for applications to beam combining. His work in these areas has resulted in coauthorships on two patents and numerous publications.

Frederick J. O'Donnell received the A.S. degree in engineering technology from Lincoln College, Northeastern University, Boston, MA, in 1977.

He joined the Lincoln Laboratory, Massachusetts Institute of Technology, Lexington, in 1973. He is currently an Assistant Staff Member in the Electro-Optical Materials and Devices Group. He has worked on process development, fabrication, testing, and packaging of a variety of III-V semiconductor optoelectronic devices, most recently on Geiger-mode avalanche photodiodes for single-photon-detection applications.

Douglas C. Oakley received the B.A. degree in physics from the University of Maine, Orono, in 1991, and the M.S. degree in physics with a concentration in optics, specifically laser design and applications, from the University of Massachusetts, Lowell, in 1996. His thesis entailed photoluminescence characterization of InP-based multiple quantum-well structures, grown at MIT Lincoln Laboratory by MBE.

In the Fall of 1996, he joined MIT Lincoln Laboratory, Electro-Optical Materials and Devices Group, as Assistant Research Staff, working on the growth of novel GaSb-based materials by OMVPE for the Thermophotovoltaics research effort. In February of 2001, he was reassigned to run the InP-based OMCVD materials' growth effort, producing novel InP/InGaAs/InGaAsP-based APD, PIN, Laser, and Modulator structures. In 2003, got promoted to Associate Technical Staff. He was part of the Mars Laser Communications Demonstration Team that was awarded the "MIT Lincoln Laboratory 2005–2006 Team Award." He was awarded the 2008 Electrochemical Society "Best Paper Award" for a coauthored work on 150 mm InP to Silicon Direct Wafer Bonding for Silicon Photonics Integrated Circuits. He is the part of the team working on Geiger-Mode Avalanche Photodiode Focal Plane Arrays recently selected as one of "R&D 100 Award" winners.

Antonio Napoleone, photograph and biography not available at the time of publication.

Jonathan Klamkin received the B.S. degree in electrical and computer engineering from Cornell University, Ithaca, NY, in 2002, M.S. degree in electrical and computer engineering, and Ph.D. degree in electronic materials from the University of California, Santa Barbara, (UCSB), in 2004 and 2008, respectively. At the UCSB, he worked on design, growth, fabrication, and characterization of widely-tunable semiconductor lasers, photodetectors, optical intensity and phase modulators, and semiconductor optical amplifiers for InP-based photonic integrated circuits with emphasis on high power photodiodes and novel coherent integrated receivers for highly linear microwave photonic links.

In 2008, he joined the Electrooptical Materials and Devices Group at MIT Lincoln Laboratory, Lexington, MA, where he is a Technical Staff Member. His current research interests include microwave photonic subsystems, high power photodiode arrays, photonic integration techniques including quantum-well intermixing for novel integrated circuits and devices, photonic integrated circuits for free-space laser communications, directly modulated frequency stabilized high-power lasers, and GaN-based optical modulators. He has presented invited talks and received two Best Paper Awards at leading conferences, has served on a number of technical program committees for leading international conferences, and has authored or coauthored more than 60 papers.

Juliet T. Gopinath received the B.S. degree in electrical engineering, in 1998, from the University of Minnesota, and the S. M. and Ph.D. degrees in electrical engineering and computer science, in 2000 and 2005, respectively, from the Massachusetts Institute of Technology (MIT), Cambridge.

From 2005 to 2009, she worked as a Member of Technical Staff at MIT Lincoln Laboratory, Lexington, MA. Her works included wavelength-beam combining of eyesafe diode arrays, cryogenic Yb:YAG lasers/amplifiers, modelocked semiconductor optical waveguide lasers (SCOWLs), high power eyesafe laser sources, and Raman spectroscopy. She is now an Assistant Professor at the University of Colorado, Boulder, in the Electrical, Computer, and Energy Engineering Department. Her research interests include ultrafast solid-state fiber lasers, semiconductor lasers, wavelength beam combining, spectroscopy, nonlinear processes in fibers, mid-infrared sources, and high-power lasers. She has authored or coauthored 23 journal papers and more than 30 conference proceedings. She is the recipient of the National Science Foundation (NSF) Graduate Fellowship (1998–2001) and the LEOS Graduate Student Fellowship (2003).

Dr. Gopinath is a member of OSA and the IEEE Photonics Society.

Daniel J. Ripin received the B.S. degree in physics from Emory University, Atlanta, GA, in 1995, and Ph.D. degree in physics from the Massachusetts Institute of Technology, Cambridge, in 2002. His dissertation research focused on the areas of ultrafast optics, photonic crystals, and integrated optics.

He is the Assistant Leader of the Laser Technology and Applications Group at MIT Lincoln Laboratory, Lexington, MA. Since 2002, at MIT Lincoln Laboratory, his research has been in the areas of high-average-power laser development, ultrafast optics, and spectroscopy.

Dr. Ripin is a member of the Optical Society of America (OSA).

Sangyoun Gee received the Ph.D. degree in physics from the Center for Research and Education in Optics and Lasers (CREOL), University of Central Florida, Orlando, in 2000.

He is currently teaching at the Gwangju Institute of Science and Technology, Korea. His areas of research include studies of the mode-locked operation, ultrafast pulse generation, high-power pulse amplification of semiconductor lasers, and low-noise pulse generation and their application.

Peter J. Delfyett (S'79–M'94–SM'96–F'02) received the B.S. degree from the City College of New York, in 1981, the M.S. degree from the University of Rochester, NY, in 1983, both in electrical engineering, and the M.Phil and Ph.D. degrees from the City University of New York, in 1987 and 1988, respectively.

He is the University of Central Florida Trustee Chair Professor of Optics, ECE and Physics at The College of Optics and Photonics, and the Center for Research and Education in Optics and Lasers (CREOL) at the University of Central Florida, Orlando. Prior to this, he was a Member of the Technical Staff at Bell Communications Research, from 1988–1993, where he concentrated his efforts toward generating ultrafast high-power optical pulses from semiconductor diode lasers, for applications in applied photonic networks. Some of his technical accomplishments were the development of the world's fastest, most powerful mode-locked semiconductor laser diode, the demonstration of an optically distributed clocking network for high-speed digital switches and supercomputer applications, the development of the lowest ever timing jitter from a mode-locked diode laser, and breaking the terabit per second data rate barrier from a single semiconductor laser. He has published more than 500 articles in refereed journals and conference proceedings and has been awarded 30 United States Patents.

Prof. Delfyett is a Fellow of the Optical Society of America (OSA), Fellow of IEEE LEOS, and has served as member of the Board of Governors of IEEE-LEOS and the Board of Directors of the OSA. Dr. Delfyett has been awarded the National Science Foundations Presidential Faculty Fellow Early Career Award for Scientists and Engineers, which is awarded to the Nations top 20 young scientists. He has also received the University of Central Florida's 2001 Pegasus Professor Award, which is the highest honor awarded by the University. Most recently, he has been awarded the Edward Bouchet Award from the American Physical Society. He has served as Editor-in-Chief of the IEEE Journal of Selected Topics in Quantum Electronics, Associate Editor of the IEEE Photonics Technology Letters, and Executive Editor of the IEEE LEOS Newsletter.

Joseph P. Donnelly (S'60–M'63–SM'88–F'90–LF'05) received the Bachelor's degree in electrical engineering from Manhattan College, Bronx, NY, and M.S. and PhD. degrees in electrical engineering from Carnegie Mellon University, Pittsburgh, PA.

He is a Senior Staff Member at Lincoln Laboratory, Massachusetts Institute of Technology, Lexington. Before joining Lincoln Laboratory, he was a NATO Post-doctoral Fellow at Imperial College, London, U.K. In addition to his position at Lincoln, he is an Adjunct Professor in the Physics Department at the University of Massachusetts Lowell. His current interests include high-power semiconductor lasers, integrated optics, and avalanche photodiodes. He is the author or coauthor of three book chapters and more than 200 journal articles.

Prof. Donnelly is a member of The Bohmesche Physical Society, Eta Kappa Nu, and Sigma Xi. He was a National Lecturer for the IEEE Electron Devices Society, in 1979. In 2001, he was a Guest Associate Editor for a special issue of the IEEE Journal of Selected Topics in Quantum Electronics on Semiconductor Lasers, and from 2002–2004, he was an Associate Editor of the IEEE Journal of Quantum Electronics.